IMPERIAL COLLEGE LONDON

Department of Earth Science and Engineering

Centre for Petroleum Studies

Upscaling Low Salinity Waterflooding in Heterogeneous Reservoirs

By

Pongpat Hongtong

A report submitted in partial fulfilment of the requirements for
the MSc and/or the DIC

September 2013

DECLARATION OF OWN WORK

I declare that this thesis “Upscaling Low Salinity Waterflooding in Heterogeneous Reservoirs” is entirely my own work and that where any material could be construed as the work of others, it is fully cited and referenced, and/or with appropriate acknowledgement given.

Signature:

Name of student: Pongpat Hongtong
Name of supervisor: Ann H. Muggeridge

ABSTRACT

Low salinity waterflooding is an Enhanced Oil Recovery (EOR) technique in which the low salinity water is injected into reservoirs containing high salinity connate water to displace oil. It increases the oil recovery as the injected low salinity water makes an initially oil/mixed wet reservoir more water wet. This is modelled by changing relative permeability as a function of salinity in the reservoir. To model this properly, a very fine grid model is required. In field scale flow simulations, this is not possible as it is very time consuming so an approach to describe this salinity-dependent waterflood development in a coarse grid model is necessary. This study demonstrates the performance of two-phase upscaling in combination with upscaling of the salinity thresholds that control low/high salinity response during secondary low salinity waterflooding in reservoirs with simple realisations of heterogeneity.

The simulations of low salinity waterflooding were performed on 1D, 2D, and 3D rectangular models of homogeneous and layered reservoirs by using the low salinity option in Eclipse. The low and high salinity-dependent relative permeabilities were upscaled using the pore volume-weighted (PVW) method, and an analytical method based on Buckley-Leverett theory. The salinity-dependent thresholds for the upscaled models were modified by comparing the salt concentration profiles of the fine and coarse grid models to determine the location where the low salinity effect occurs. The performance of the upscaling methods is mainly focused on reproduction of fine-grid oil recovery and water breakthrough.

The results show that the PVW pseudo-relative permeabilities can compensate for numerical dispersion in the coarse-grid low salinity waterflood models more effectively, and the match between the fine-grid and coarse-grid solution can be further improved by using modified salinity thresholds. However, the effect of pseudo-salinity thresholds on low salinity waterflood modelling in the layered models seems to be less significant. The drawback of the PVW pseudos is a large number of sets of pseudos are required to achieve accurate results. Using the analytically derived pseudos with appropriate pseudo salinity thresholds could be more feasible as it is more manageable and can give comparable results in some cases.

ACKNOWLEDGEMENTS

I wish to thank my Imperial College supervisor, Prof. Ann H. Muggeridge for support and guidance, without which this project would not have been possible. I also wish to thank my family for their love and encouragement throughout the year. Thanks are extended to the academic staffs and my colleagues of MSc Petroleum Engineering for their support and friendship, and to my company, PTT Exploration and Production, for financial support.

TABLE OF CONTENTS

LIST OF FIGURES

LIST OF TABLES

Imperial College London

Upscaling Low Salinity Waterflooding in Heterogeneous Reservoirs

Pongpat Hongtong

Imperial College Supervisor: Professor Ann H. Muggeridge

Abstract

Low salinity waterflooding is an Enhanced Oil Recovery (EOR) technique in which the low salinity water is injected into reservoirs containing high salinity connate water to displace oil. It increases the oil recovery as the injected low salinity water makes an initially oil/mixed wet reservoir more water wet. This is modelled by changing relative permeability as a function of salinity in the reservoir. To model this properly, a very fine grid model is required. In field scale flow simulations, this is not possible as it is very time consuming so an approach to describe this salinity-dependent waterflood development in a coarse grid model is necessary. This study demonstrates the performance of two-phase upscaling in combination with upscaling of the salinity thresholds that control low/high salinity response during secondary low salinity waterflooding in reservoirs with simple realisations of heterogeneity.

The simulations of low salinity waterflooding were performed on 1D, 2D, and 3D rectangular models of homogeneous and layered reservoirs by using the low salinity option in Eclipse. The low and high salinity-dependent relative permeabilities were upscaled using the pore volume-weighted (PVW) method, and an analytical method based on Buckley-Leverett theory. The salinity-dependent thresholds for the upscaled models were modified by comparing the salt concentration profiles of the fine and coarse grid models to determine the location where the low salinity effect occurs. The performance of the upscaling methods is mainly focused on reproduction of fine-grid oil recovery and water breakthrough.

The results show that the PVW pseudo-relative permeabilities can compensate for numerical dispersion in the coarse-grid low salinity waterflood models more effectively, and the match between the fine-grid and coarse grid solution can be further improved by using modified salinity thresholds. However, the effect of pseudo-salinity thresholds on low salinity waterflood modelling in the layered models seems to be less significant. The drawback of the PVW pseudos is a large number of sets of pseudos are required to achieve accurate results. Using the analytically derived pseudos with appropriate pseudo salinity thresholds could be more feasible as it is more manageable and can give comparable results in some cases.

Introduction

Low salinity waterflooding is an EOR technique which increases the oil recovery by injecting low salinity water instead of the high salinity water usually used in conventional waterflooding. Several experimental and field studies (Tang and Morrow, 1997; Lager et al., 2006) have shown that the salinity of water affects the reservoir properties in some way causing changes in oil displacement efficiency. The idea of varying the injected brine composition to improve the oil recovery was first introduced by Yildiz and Morrow (1996) after their experiments on Berea sandstone core samples with Moutray crude oil. The study by Tang and Morrow (1997) supports this idea by showing that lowering the salinity of either connate water or injected brine can increase the oil recovery. They also suggested that the waterflood recovery is improved because of a change in wettability toward water wet when the salinity of water in reservoirs decreases. This change results in lower residual oil saturation, lower water relative permeability (k_{rw}) and higher oil relative permeability (k_{ro}) at any given water saturation (S_w). These test results showed that conventional waterflood efficiency can be improved by up to 38% by using low salinity water (Jerauld et al., 2006). The mechanisms for increasing oil recovery by low salinity waterflooding have been investigated by several studies. Recently, Lager et al. (2006) concluded that the liberation of additional oil is caused by reduction in ion binding between oil and rock, which is a result of low salinity-induced multicomponent ion exchange.

One important characteristic of low salinity waterflooding is that the injected brine displaces the connate water causing connate water banking. This behaviour was first identified by Russell et al. (1947), who showed that in their waterflood experiments about 80% of connate water was produced after the water was injected for 1 pore volume. Thus, the salinity of produced water in low salinity waterflooding begins at connate salinity and reduces to injected brine salinity. However, some evidence (Salter and Mohanty, 1982) suggests that the displacement of the connate water in the pore space by the injected water is not as completely pistonlike as is predicted analytically. This is because the two types of water mix to some extent. In addition, Jerauld et al. (2006) suggested, based on experimental studies, that the level of incremental oil recovery by low salinity waterflooding depends on the salinity but only in a certain range. Many test results (McGuire et al., 2005; Webb et al., 2005) demonstrated no production benefit was found when the salinity of water is above 7,000 ppm but that additional recovery was achieved when the salinity was reduced further. In addition, some data (Tang and Morrow, 1997; Jerauld et al., 2006) indicated the difference in additional recovery achieved when the salinity was reduced below 1,250 ppm is subtle.

In reservoir modelling, the best grid resolution to capture physical dispersion whilst minimising numerical dispersion (and thus properly capture the mixing of low and high salinity water) is quite large and so may require a very long time to run. For

field scale simulations, the reservoir model is, therefore, usually coarsened to reduce the number of grid cells so the flow simulation model requires less computer time. The single-phase properties such as porosity, net-to gross and absolute permeability (k) are then upscaled to obtain average properties for the coarse grid. Grid coarsening normally causes numerical dispersion problems, which may not be important when modelling single-phase flow. The study by Jerauld et al. (2006) shows that the physical dispersion can be approximately modelled in 1D and 2D areal simulations by using numerical dispersion. He also suggested the number of grid blocks between an injector and a producer should be about 10 as it corresponds to 2-5% dispersivity level, which was considered appropriate to use in simulations (Mahadevan et al., 2002). In two-phase flow this numerical dispersion causes smearing of saturation fronts resulting in early water breakthrough because water flows out of the grid block at the water saturation less than shock-front water saturation (S_{wf}) if the rock relative permeability curve is used.

A further problem with grid coarsening is that it means that reservoir heterogeneity may not be properly resolved. This may mean that the coarse grid simulations may not correctly model the correct multi-phase flow behaviour particularly if the correlation length of heterogeneity is close to the coarse grid length, for example, thin, high permeability layers and extensive, thin shale barriers (Barker and Thibeau, 1997). These kinds of heterogeneity cause non-uniform water saturation which will also cause non-uniform salt concentration in low salinity flooding, which in turn may mean that coarse grid models do not predict the correct behaviour. The usual approach in these cases is to upscale both absolute and relative permeabilities. The study by Christie and Blunt (2001) showed that just upscaling absolute permeability can result in some discrepancies between the coarse-grid and fine-grid solutions of waterflood simulation.

In this case, multiphase upscaling such as relative permeability upscaling becomes necessary to compensate both for sub-grid scale heterogeneity (homogenisation) and numerical dispersion (pseudoisation). Several pseudoisation techniques have been developed; however, the analysis of dynamic pseudo-relative permeability methods by Barker and Dupouy (1996) shows there is no ideal method that can reproduce the fine-grid solution precisely for every case. In low salinity waterflooding upscaling, Jerauld et al. (2006) demonstrated the use of pseudo-salinity thresholds by modifying the upper and lower salinity-dependent thresholds but did not discuss upscaling the relative permeabilities. Their results indicated that using only threshold upscaling could approximate the fine-grid behaviour in the coarse-grid model effectively.

The objective of this study is to evaluate the benefits from using two-phase upscaling in conjunction with threshold upscaling to compensate for numerical dispersion during the simulation of secondary low salinity waterflooding in reservoirs with simple realisation of heterogeneity. Two pseudo-relative permeability methods, one numerical and one analytical, combined with a modification of salinity-dependent thresholds are considered in this study.

Methodology

This study uses synthetic data from an Eclipse example data file for low salinity waterflooding. The low and high salinity-dependent oil/water relative permeability curves are shown in Fig.1. These relative permeability curves were used in all the simulation studies reported in this work. From the graph, the residual oil saturation (S_{or}) and irreducible water saturation (S_{wc}) are lower in low salinity system resulting in higher oil recovery.

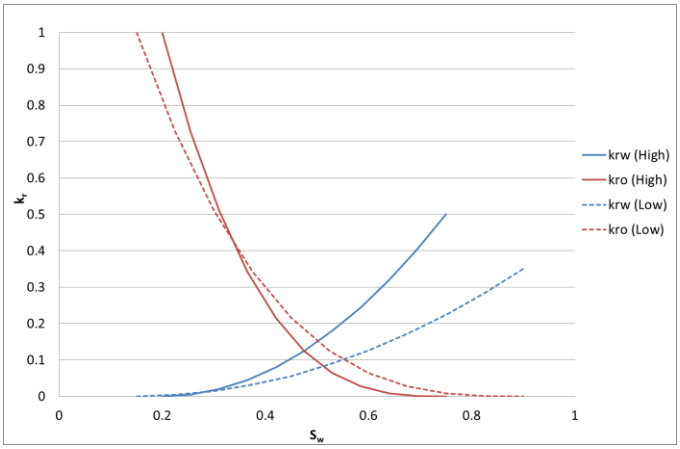

Fig.1 Rock relative permeability curve for high and low salinity systems

A Buckley-Leverett analysis was also performed to determine shock-front water saturation for a standard waterflood in the separate high and low salinity systems, and also when low salinity water is injected into a reservoir with high salinity connate water. These analytic results were compared with the 1D fine-grid simulation results to evaluate whether the models can produce the correct behaviour with a suitable fine-grid resolution. The simulation studies were performed in 1D, 2D and 3D on fine and coarse grid models. The low salinity waterflood simulations were modelled by using the low salinity option in Eclipse 100 (Schlumberger, 2010), which allows the relative permeabilities to be modified as a function of the salt concentration by interpolation as:

$$k_{rw} = F_1 k_{rw}^L + (1 - F_1) k_{rw}^H \qquad \text{(Eq. 1)}$$

$$k_{ro} = F_1 k_{ro}^L + (1 - F_1) k_{ro}^H \qquad \text{(Eq. 2)}$$

where k_{rw} and k_{ro} are the water and oil relative permeability respectively, the index *L* stands for high salinity, the index *H* stands for low salinity, and the weighting factor F_1 is a fuction of salt concentration. At the lower salinity threshold, F_1 equals 1 and at the upper threshold equals 0. The values in between were calculated by linear interpolation. The salinity of connate water used in low salinity waterflood simulation is 30,000 ppm while that of injected brine is 1,000 ppm. The low and high salinity threshold in fine grid was assumed to be 1,000 and 7,000 ppm, respectively.

In the coarse-grid models, upscaled properties such as pseudo-relative permeabilities (pseudos) and pseudo-salinity thresholds (denoted by *T*) are applied. The oil and water relative permeabilities of low and high salinity system were upscaled using the pore-volume weighted (PVW) method (Intera Information Technologies, 1994), which varies from the Kyte and Berry method (Kyte and Berry, 1975) in that it uses pore volume weighting to calculate the average pressure. The pseudos were generated by the PSEUDO package. The pseudos calculated from the upscaling method introduced by Muggeridge (2007) (based on Buckley-Leverett theory, see Appendix C), which uses truncation of k_{rw} at S_w<S_{wf}, and changing k_{ro} to maintain the total mobility, were also applied. The pseudo-salinity thresholds were obtained by comparing the salt concentration profiles of the fine-grid and the coarse-grid model to determine the location in coarse-grid models where the low salinity effect occurs (Muggeridge, 2007, see Appendix E). This discrepancy between the salinity profiles is also a result of numerical dispersion in coarse-grid models.

From the simulation results, oil recovery water cut, salt production, and pressure drop between the wells were observed in the fine-grid and coarse-grid models to evaluate the performance of two-phase upscaling. The10-grid model suggested by Jerauld et al. (2006) was also examined in the 1D and 2D simulations of homogeneous reservoirs for comparison.

1D Simulation

A sector model of homogeneous reservoir with 20% porosity and permeability of 100 mD was used in the 1D simulation. The reservoir and fluid properties were summarised in Table 1. One production and one injection well were set to perform secondary low salinity waterflooding with the injection and production rates of 304 sm^3/day. This gives the velocity of the water front approximately 2 ft/day. The distance between the injector and the producer was fixed at 1 km. The fine-grid model has 96 grid cells excluding the injection and the production well block while the coarse-grid model has 3 grid cells. The sizes of the injection and the production well block in the fine-grid, 10-grid and coarse-grid model are constant to maintain the well locations and to avoid near-well region well upscaling (Ding and Renard, 1994). Thus, the rock curves were applied to the well blocks in all cases in this study.

Firstly, the fine-grid standard waterflood simulation, which uses the same salinity for the injected water and the connate water, was conducted in the high salinity (30,000 ppm) and low salinity (1,000 ppm) systems. This was required for generating the high and low salinity pseudo curves. The low salinity waterflood simulation was then run without upscaling in the fine-grid, 10-grid, and coarse-grid models until the injection volume equals to 1.5 pore volume (PV). The water saturation profiles of the fine-grid standard and low salinity waterflood simulations were compared with the Buckley-Leverett analysis results. The block salt concentrations in the fine-grid and the coarse-grid low salinity waterflood model were plotted to determine the pseudo-salinity thresholds. The salinity thresholds of 1,000 and 7,000 ppm were changed to 3,700 and 10,700 ppm. The coarse-grid model was run with 2 sets of the pseudos (PVW and B-L approximation methods) and/or the pseudo-salinity thresholds.

2D Simulation for Homogeneous System

The simulations were performed on a quarter 5-spot pattern model and a vertical cross-section model with an injector and producer pair to observe the performance of relative permeability and salinity threshold upscaling on macroscopic sweep modelling. The sizes of the well blocks in all cases were constant, and the reservoir and fluid properties used in the models were summarised in Table 1. The standard waterflood simulations were run only on the fine-grid model for pseudo generation.

Quarter 5-spot pattern model

A sector model of 1×1 km^2 with the thickness of 50 m was generated. The number of fine-grid blocks is 98×98 while the coarse-grid model has 5×5 grid cells (Fig.2). The injection and production rates were controlled at 1,900 sm^3/day until 1.5 PV injected to give the velocity of water front at the cross sectional area perpendicular to the velocity at the mid-point between the wells approximately 1 ft/day. The salinity thresholds were changed to 6,800 and 14,200 ppm in the upscaled models.

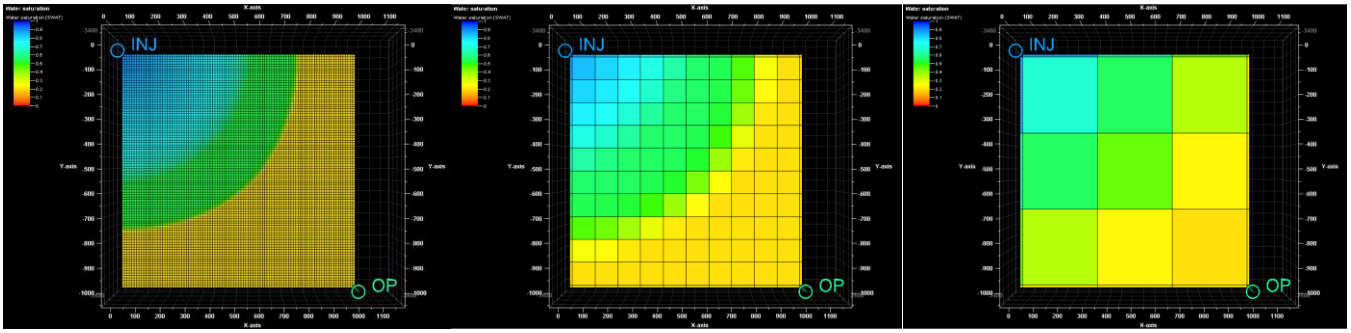

Fig.2 Homogeneous quarter 5-spot pattern models showing water saturation profile (fine-grid, 10-grid and coarse-grid without upscaling)

Vertical cross-section model

A reservoir model of 1-km length and 50-m thickness was generated. The model was divided into 50 layers for the fine-grid model and 10 layers for the 10-grid and coarse-grid models. The number of grid cells between the injector and the producer is 96 for the fine-grid and 3 for the coarse-grid model (Fig.3). The injection and production rates were controlled at 167 sm^3/day, which gives the velocity of water front approximately 1 ft/day. For the upscaled models, the salinity thresholds were changed to 4,500 and 10,200 ppm.

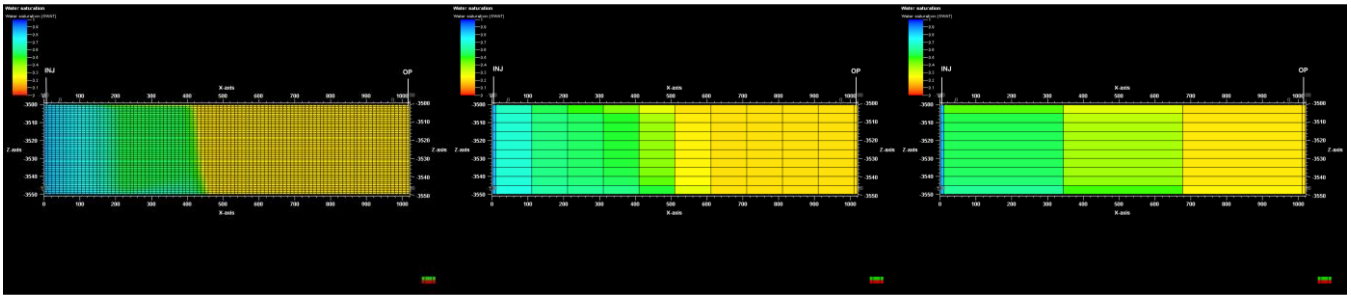

Fig.3 Homogeneous vertical cross-section models showing water saturation profile with slight slumping of the water flow due to gravity (fine-grid, 10-grid and coarse-grid without upscaling)

Table 1 – Reservoir and fluid properties for homogeneous reservoir models

Properties	1D Models	2D Quarter 5-spot Models	2D Vertical X-section Models	Unit
Dimension (x × y)	1,020×100	1,020×1,020	1,020×100	m
Thickness (z)	50	50	50	m
Injector location (i, j, k)	1, 1, 1	1, 1, 1	1, 1, 1	
	98, 1, 1 (fine grid)	98, 98, 1 (fine grid)	98, 1, 1 (fine grid)	
Producer location (i, j, k)	12, 1, 1 (10 grid)	12, 12, 1 (10 grid)	12, 1, 1 (10 grid)	
	5, 1, 1 (coarse grid)	5, 1, 1 (coarse grid)	5, 1, 1 (coarse grid)	
Porosity	0.2	0.2	0.2	
Horizontal Permeability	200	200	200	mD
Vertical Permeability	-	-	20	mD
Initial Reservoir pressure	270	510	510	bara
Rock compressibility	0.3×10^{-5} at 270 bara	0.3×10^{-5} at 270 bara	0.3×10^{-5} at 270 bara	$bara^{-1}$
Water compressibility	4.6×10^{-5} at 270 bara	4.6×10^{-5} at 270 bara	4.6×10^{-5} at 270 bara	$bara^{-1}$
Oil density	850	850	850	kg/m^3
Water density	1,000	1,000	1,000	kg/m^3
Oil viscosity	0.47	0.47	0.47	cP
Water viscosity	0.5	0.5	0.5	cP
Oil formation volume factor	0.999 at 280 bara	0.999 at 280 bara	0.999 at 280 bara	rm^3/sm^3
Water formation volume factor	1.03 at 270 bara	1.03 at 270 bara	1.03 at 270 bara	rm^3/sm^3
Connate salinity	30,000	30,000	30,000	ppm

2D Simulation for Heterogeneous System

A vertical cross-section model of different-permeability layered reservoir was used to represent flow in the high permeability streak, which causes early water breakthrough. The dimensions and number of cells in the fine-grid model are the same as the homogeneous vertical cross-section model. The model has 3 layers with the top and bottom layers of 100 mD, and the middle layer of 500 mD. The fine-grid model was homogenised to be a 1D model with 5 grid blocks as shown in Fig.4. The sizes of the well blocks were kept constant. The absolute permeability, which is upscaled from the fine-grid model using arithmetic averaging, becomes 220 mD. The other model parameters were provided in Table 2. The reservoir production and injection rates were controlled at 167 sm^3/day similarly to the 2D homogeneous model. Four sets of pseudo-salinity thresholds were used due to different salt concentration profiles in the low and high permeability layer of the fine-grid model. The approximation of these pseudo thresholds was explained in the result section. These pseudo-salinity thresholds were applied to the upscaled models with the PVW pseudos only. All simulations were run until 1.5 PV injected.

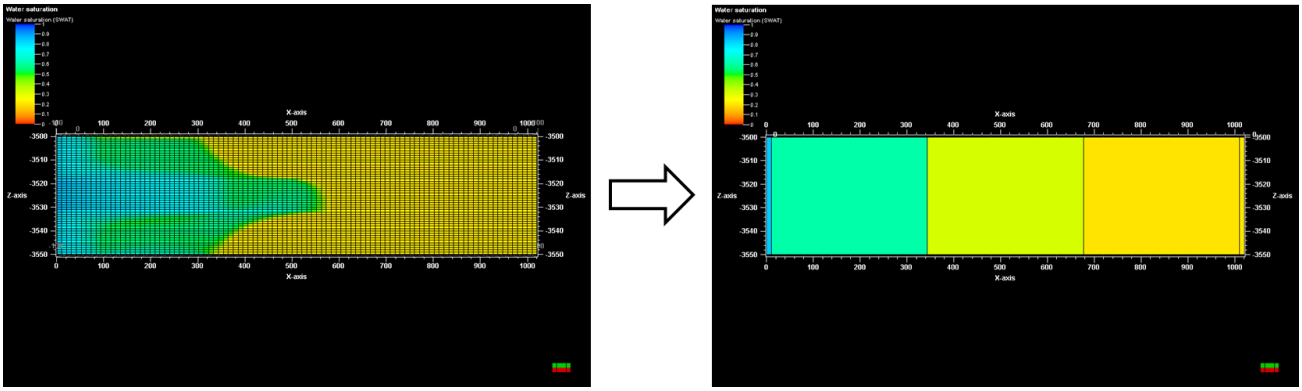

Fig.4 Homogenisation of 2D layered model showing water saturation profile

3D Simulation for Heterogeneous System

A layered model of 1×1×0.05 km^3 with an injector and producer pair was used in this study. The fine-grid model has 98 grid blocks in x and y-axis, and 50 grid blocks in z-axis, which were grouped into the same 3 layers as the 2D layered model. The fine-grid model was homogenised and coarsened to 5×5×1 grid blocks (Fig.5). As a result, this model behaves as a 2D quarter 5-spot pattern model. The model has an absolute permeability of 220 mD, which was upscaled from the fine-grid model using arithmetic averaging. The sizes of the well blocks in the fine-grid and coarse-grid models were maintained constant. The other model parameters were provided in Table 2. The upscaled model was run with 2 types of pseudo-relative permeabilities, and 4 sets of pseudo-salinity thresholds determined similarly to those of the 2D layered model. The injection and production rates were controlled at 1,210 sm^3/day to give the water front velocity at the cross sectional area perpendicular to the flow at the mid-point between the wells approximately 0.5 ft/day. The results were observed until 1 PV injected.

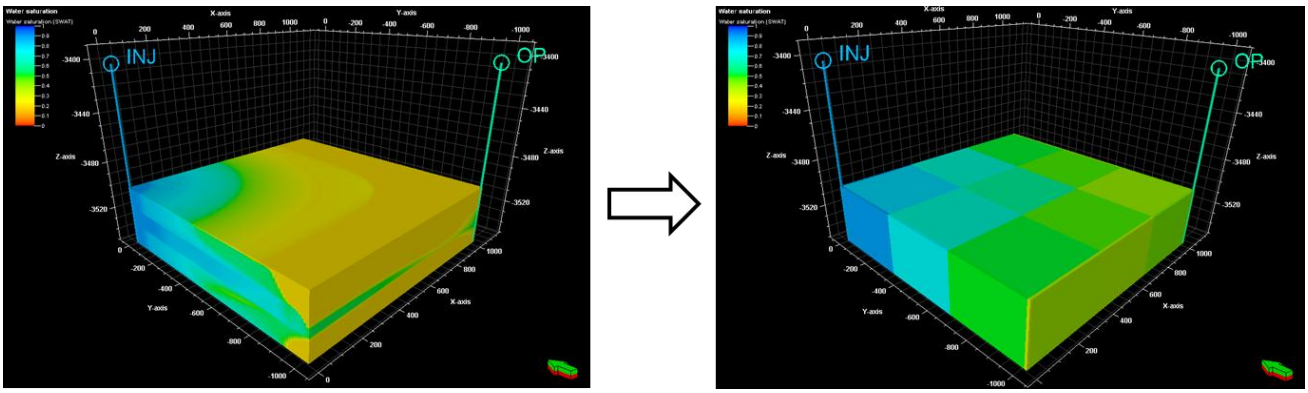

Fig.5 Homogenisation of 3D layered model showing water saturation profile

Table 2 – Reservoir and fluid properties for layered reservoir models

Properties	2D Models	3D Models	Unit
Dimension (x × y)	1,020×100	1,020×1,020	m
Thickness (z)	50	50	m
Injector location (i, j, k)	1, 1, 1	1, 1, 1	
Producer location (i, j, k)	98, 1, 1 (fine grid)	98, 98, 1 (fine grid)	
	5, 1, 1 (coarse grid)	5, 5, 1 (coarse grid)	
Porosity	0.2	0.2	
Horizontal permeability	100/500 (fine grid)	100/500 (fine grid)	mD
	220 (coarse grid)	220 (coarse grid)	
Vertical permeability	10/50 (fine grid)	10/50 (fine grid)	mD
	13.16 (coarse grid)	13.16 (coarse grid)	
Initial Reservoir pressure	510	510	bara
Rock compressibility	0.3×10^{-5} at 270 bara	0.3×10^{-5} at 270 bara	$bara^{-1}$
Water compressibility	4.6×10^{-5} at 270 bara	4.6×10^{-5} at 270 bara	$bara^{-1}$
Oil density	850	850	kg/m^3
Water density	1,000	1,000	kg/m^3
Oil viscosity	0.47	0.47	cP
Water viscosity	0.5	0.5	cP
Oil formation volume factor	0.999 at 280 bara	0.999 at 280 bara	rm^3/sm^3
Water formation volume factor	1.03 at 270 bara	1.03 at 270 bara	rm^3/sm^3
Connate salinity	30,000	30,000	ppm

Results

Buckley-Leverett Analysis

A Buckley-Leverett analysis was performed assuming a waterflood in which the low salinity relative permeabilities were valid and also for the case in which the high salinity relative permeabilities were assumed to be valid. In the high salinity system the shock front saturation was 0.58 (denoted by $S_{wf,h}$) whilst in the low salinity system it was 0.7 (denoted by $S_{wf,l}$). The high salinity shock also has a higher characteristic velocity than the low salinity shock indicating faster water breakthrough in the high salinity system than in the low salinity system. For the low salinity waterflood, the low salinity water is injected into a reservoir with high salinity connate water. In this case the water saturation profile shows a connate water front saturation (S_{wcf}) of 0.52 while the following injected water front saturation is 0.72.

The block water saturation in the 1D fine-grid standard and low salinity waterflood models are plotted against distance and compared with the Buckley-Leverett analysis results in Fig.6. The graphs show good consistency between the simulation and B-L analysis results for the standard waterflood models. For the low salinity waterflood, the simulation result shows $S_{wcf} < S_{wf,h}$ as predicted by the B-L curve, a connate water bank and the trailing low salinity shock. Both the leading and the trailing shocks are spread out by numerical dispersion; however, this effect is much worse for the trailing front. This is because the self-sharpening effect is less strong at higher water saturations where the range of characteristic speeds for these saturations is lower.

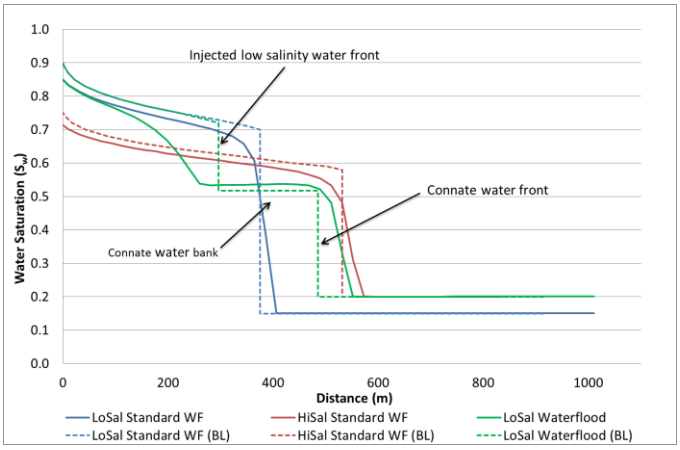

Fig.6 Water saturation profiles in 1D fine-grid standard waterflood and low salinity waterflood models

Pseudo-relative Permeability

The PVW pseudo-relative permeabilities were calculated by the PSEUDO package from the fine-grid simulations. The pseudos generated by the PVW method are different for each grid block and each flow direction. In the 1D and 2D homogenised-grid models, only oil and water pseudo-relative permeabilities in x-direction for high and low salinity systems was specifically assigned to each grid block in the coarse-grid model. Fig.7 and 8 show the example of the PVW pseudos in the separate high salinity and low salinity systems for each of the inter-well blocks in the 1D model.

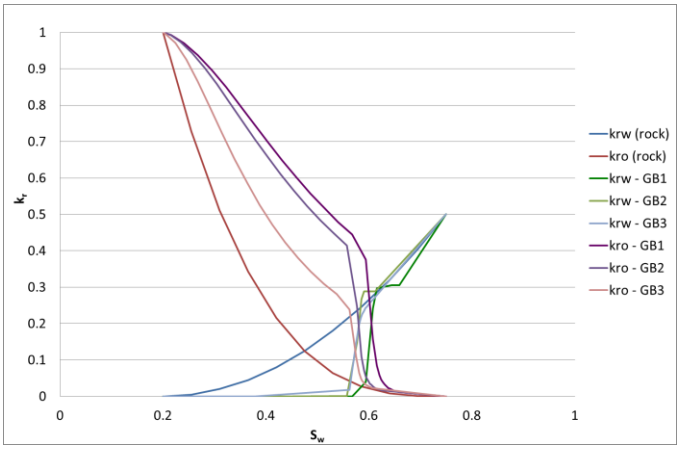

Fig.7 High salinity PVW pseudo-relative permeability curve for 1D coarse-grid model

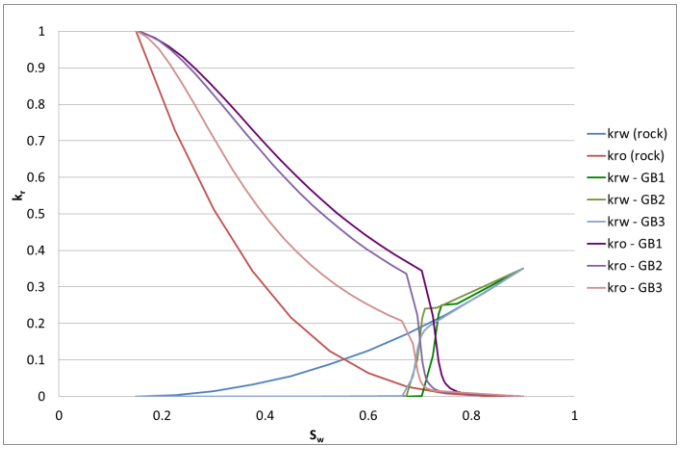

Fig.8 Low salinity PVW pseudo-relative permeability curve for 1D coarse-grid model

Typically, the PVW method produces a directional pseudo-relative permeability. Thus, two sets of the pseudos (k_{rx} and k_{ry}) should be applied to each grid block to capture the flow in x and y-directions in 2D simulations. However, this is not possible when simulating low salinity waterflooding. The pseudos were, therefore, selectively, assigned to each grid block. Fig.9 illustrates how the pseudos were assigned for each cell in the 2D quarter 5-spot pattern and 3D homogenised-grid models according to the main flow directions into adjacent cells. The pseudos of the grid cells in the diagonal line between the injector and the producer are identical in both x and y-directions. The rock curves were used in the grid blocks at the boundary in this study because their pore volumes were small. For the 2D vertical cross-section model, the pseudo-relative permeabilities in x-direction were used as the flow in z-direction normally has less impact on the overall sweep.

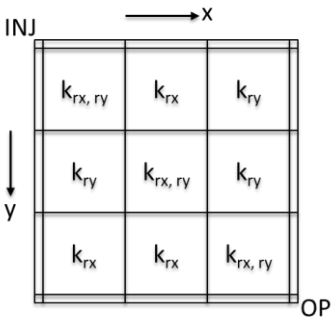

Fig.9 PVW pseudos assigned to each grid block in 2D quarter 5-spot pattern and 3D homogenised-grid models

Fig.10 and 11 show the high and low salinity pseudos for injection and non-injection well blocks obtained from the B-L approximation method (see Appendix C). The injection well pseudos were assigned to the grid blocks adjacent to the injection well block as in this block the inlet water saturation is nearly 1-S_{or}. This is due to the size of the well block in the coarse-grid model is small compared with the adjacent blocks. The non-injection well block pseudos were assigned to the remaining inter-well blocks in the coarse-grid models.

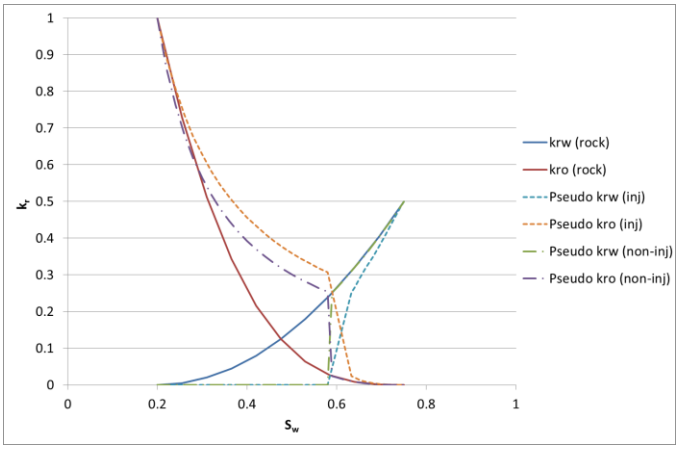

Fig.10 High salinity pseudo-relative permeability curves calculated by the B-L approximation method

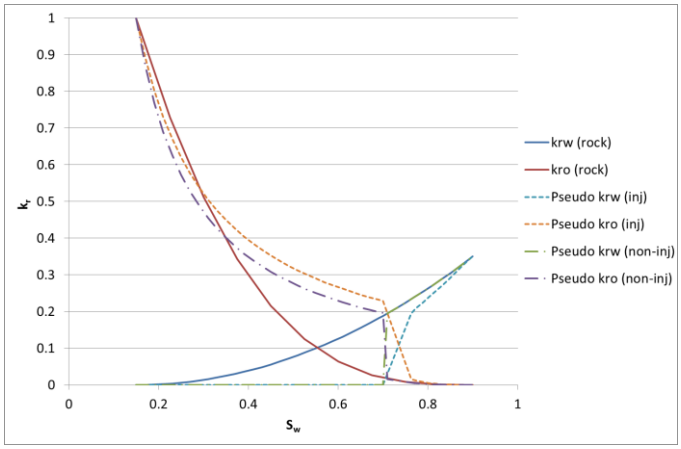

Fig.11 Low salinity pseudo-relative permeability curves calculated by the B-L approximation method

Pseudo-salinity Thresholds

In the 1D study, the salinity thresholds of 1,000 and 7,000 ppm used in the fine-grid model were changed to 3,700 and 10,700 ppm for the coarse-grid model. These were determined using the location where the salinity effect occurs when comparing the fine and coarse grid salt concentration profiles (Fig.12). For the 2D quarter 5-spot pattern model, the salinities in the diagonal grid cells between the injector and the producer were used to construct the salt concentration profiles. As a result, the salinity thresholds were changed to 6,800 and 14,200 ppm.

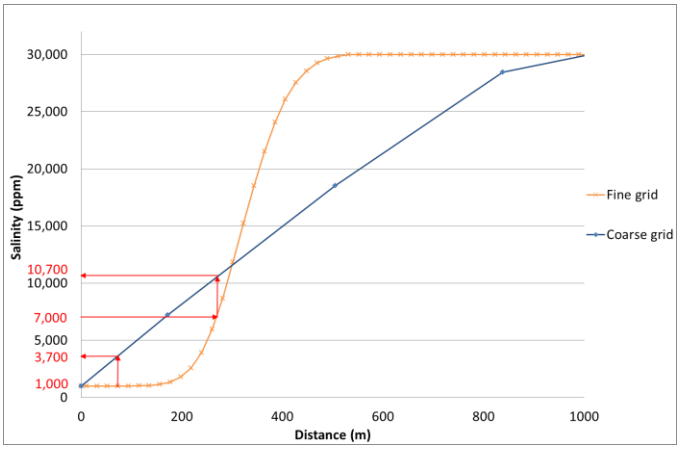

Fig.12 Estimation of pseudo-salinity thresholds by construction of salt concentration profiles for 1D model

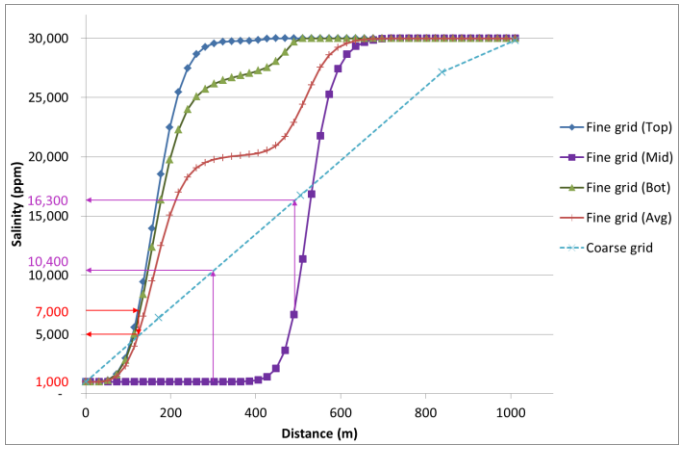

Fig.13 Estimation of pseudo-salinity thresholds by construction of salt concentration profiles for 2D homogenised-grid model

In the vertical cross-section model, the salt concentration as well as the water saturation at different depths is not uniform across the cross sectional area perpendicular to the fluid flow due to the gravity effect. Thus, the salt concentration profiles of the top, middle, and bottom layers were plotted to determine the average pseudo-salinity thresholds, which are approximately 4,500 and 10,200 ppm. For the 2D layered model, the water saturation pattern as well as the salt concentration distribution varies with rock permeability. The top and bottom, low permeability layers give pseudo-salinity thresholds in the coarse-grid model of 1,000 and 7,000 ppm (T_l) while the middle, high permeability layer gives 10,400 and 16,300 ppm (T_h) as shown in Fig 13. However, these pseudo thresholds might not accurately compensate for numerical dispersion of the salt concentration in the coarse-grid model, which uses the average absolute permeability. Two additional sets of pseudo thresholds were, therefore, generated. The first one was estimated by averaging the salinity in each column of the grid blocks in the fine-grid model (red curve in Fig.13) giving the average pseudo thresholds (T_{avg}) of 1,000 and 5,500 ppm. The other was approximated by using the upper threshold determined from the high permeability layer and the lower threshold from the low permeability layer resulting in the approximated pseudo thresholds (T_{apx}) of 1,000 and 16,300 ppm. The latter is aimed to capture the whole range of low salinity effect in the fine-grid model. In summary, 4 sets of pseudo-salinity thresholds were tested in the 2D homogenised-grid model. For the 3D model, the pseudo-salinity thresholds were estimated similarly to the 2D layered model by plotting the block salt concentrations of the homogenised diagonal grid blocks against the salinity profiles in the fine-grid model. 4 sets of pseudo thresholds used in the 3D homogenised-grid model are 2,200/6,500 ppm (T_l), 16,100/20,000 ppm (T_h), 2,200/7,000 ppm (T_{avg}), and 2,200/20,000 ppm (T_{apx}).

1D Simulation

Fig.14 shows the comparison of oil recovery factor in different grid sizes using different pseudo-relative permeabilities and pseudo-salinity thresholds. The 10-grid model gives a reasonably good prediction of ultimate recovery with about -2% error compared to the fine-grid result while the coarse-grid with no upscaling gives -6.5% error. Using the pseudo-relative permeability calculated by the PVW method improves the match between of the fine-grid and the coarse-grid model. The predicted ultimate recovery is close to that of 10-grid model. Meanwhile, the recovery predicted by the B-L approximated pseudos (denoted as *Apx* k_r in the graph) improved the match at early time before water breakthrough but the ultimate recovery is slightly higher than the original coarse-grid solution. The graphs also show that using the PVW pseudo-relative permeabilities together with the pseudo-salinity thresholds gives significant improvement in the coarse-grid results. In terms of water breakthrough time, using only the pseudo-salinity thresholds still produces early water breakthrough (Fig.15) as the numerical dispersion of the water saturation is not corrected but the problem can be compensated by the pseudo-relative permeabilities. The accurate prediction of water breakthrough time in the upscaled models may be a result of truncated pseudo-water relative permeability at $S_w<S_{wf}$, which helps reducing numerical dispersion problem in the coarse-grid models. The upscaled models also gives a good reproduction of the fine-grid maximum water cut at late times although high water cut can be observed at intermediate times for both types of pseudos.

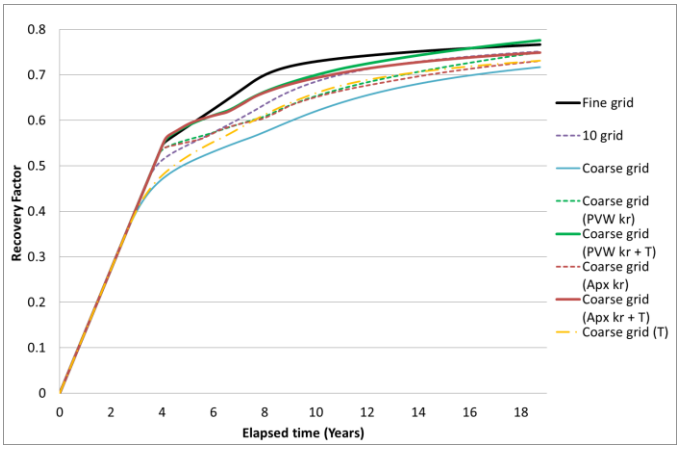

Fig.14 Effect of pseudo-k_r and salinity thresholds on oil recovery in 1D models

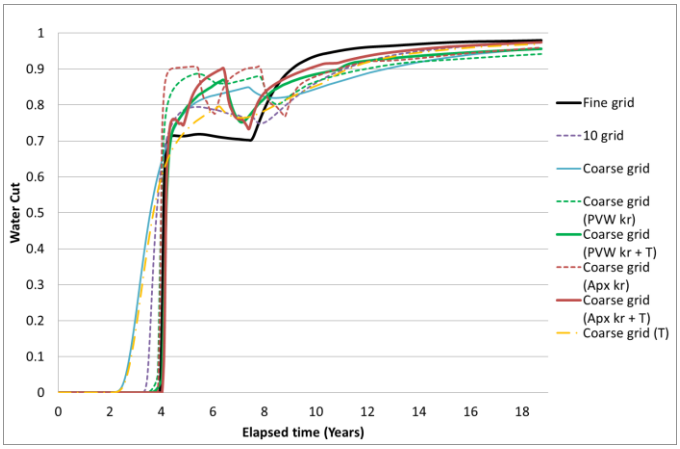

Fig.15 Effect of pseudo-k_r and salinity thresholds on water cut in 1D models

The salt production rates from different grid sizes were plotted against elapsed time in Fig.16. The graphs show a sharp drop in the salt production rate in the fine-grid model when the production well starts to produce the low salinity injected water after the connate water. The effect of numerical dispersion in the salt production in the coarse-grid models is seen in the early salt production, which corresponds to the water breakthrough. It is also shown as a gradual decrease in the salt production rate, which indicates a significant degree of mixing of the connate water and the injected water. This is confirmed by the salt concentration profile in Fig.12. Fig.16 also shows the upscaled models can predicted the maximum salt production time correctly although the maximum rate is still off. An increased pressure drop between the wells is also observed. The difference in the pressure drop in 1D model with difference grid sizes is not significant although the pseudo-relative permeability causes some decreases in pressure drop (Fig.17). This is because the pseudo oil relative permeabilities at $S_w<S_{wf}$ are much higher than the rock curve. Thus, the pressure drop decreases to maintain the same flow rate.

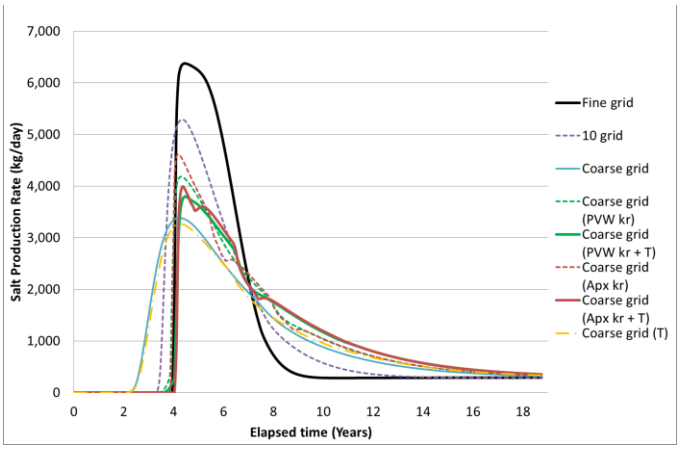

Fig.16 Effect of pseudo-k_r and salinity thresholds on salt production rate in 1D models

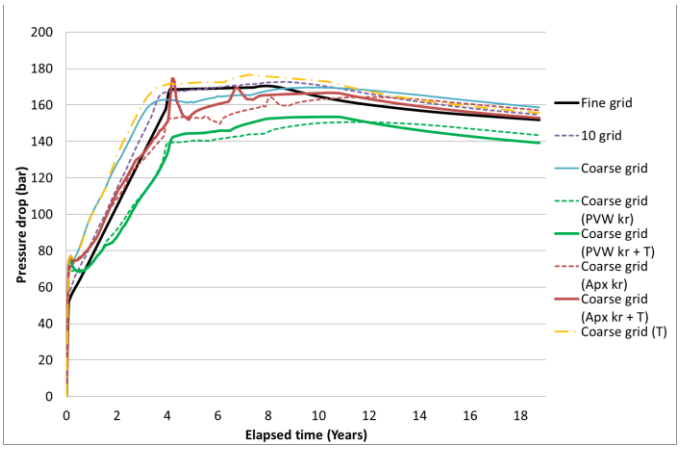

Fig.17 Effect of pseudo-k_r and salinity thresholds on pressure drop in 1D models

2D Simulation for Homogeneous System

Quarter 5-spot pattern model

The model with the PVW relative permeabilities gives a similar oil recovery prediction to the 10-grid model while the oil production from the B-L approximated pseudos behaves similarly only at early and intermediate times as shown in Fig.18. The use of pseudo-salinity thresholds still helps to improve the reproduction of the fine-grid solution in the connate water banking region resulting in higher oil recovery at intermediate times as seen in the 1D simulations. However, the recovery prediction after the water breakthrough is overestimated when the PVW pseudos and pseudo-salinity thresholds are used together whereas the result from the B-L approximated pseudos is promising. Fig.19 represents the effect of pseudos on the water cut. High water cut is still observed at intermediate times in both the models using pseudo-relative permeability. Nevertheless, the water breakthrough time is improved. With the use of pseudo-salinity thresholds, the high water cut at intermediate times is reduced but the water breakthrough is delayed, especially for the B-L approximated pseudos. A pitfall in using the PVW pseudo-relative permeability, which is a directional relative permeability, in two-phase modelling here is the pseudos cannot be assigned to the grid cells properly as mentioned in Methodology section. The upscaled model, therefore, may not be able to reproduce the flow in the fine-grid model accurately as in 1D model. Thus, these results may not exactly represent the actual effect of using the PVW pseudo-relative permeabilities. In contrast, the errors from the pseudos calculated from the B-L approximation are possibly due to the method is based on the assumption of 1D linear flow, which might not be able to sufficiently represent the actual flow behaviour in the 2D model. The characteristics of salt production profile in the fine-grid, coarse-grid and upscaled models are similar to that of the 1D models.

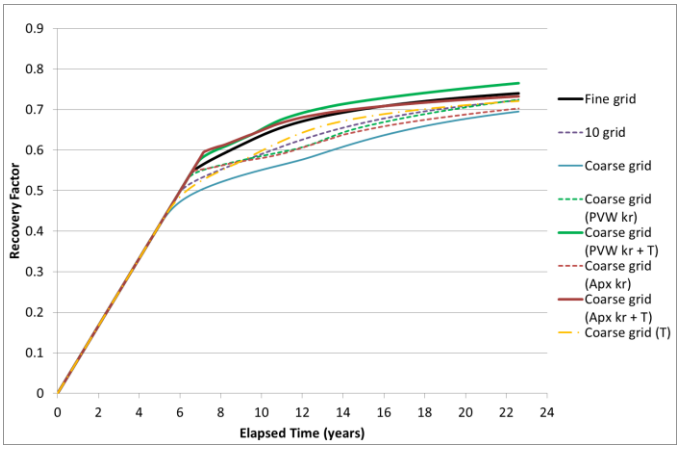

Fig.18 Effect of pseudo-k_r and salinity thresholds on oil recovery in 2D quarter 5-spot pattern models

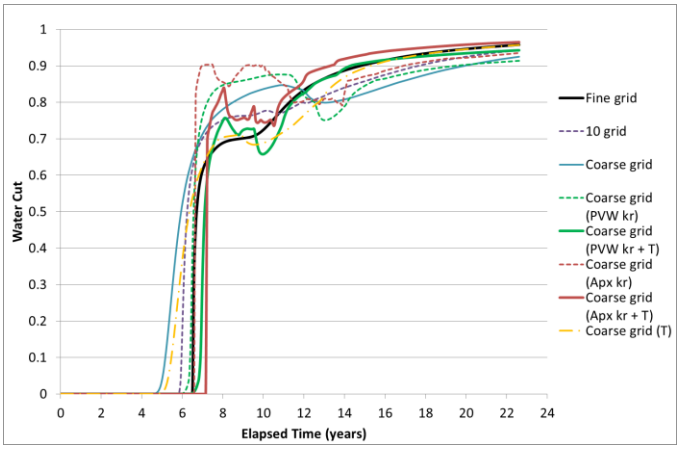

Fig.19 Effect of pseudo-k_r and salinity thresholds on water cut in 2D quarter 5-spot pattern models

With the configuration of the grid blocks used in the models that maintains the size of the well blocks, the pressure drop between the wells is 50% higher in the 10-grid model than the fine-grid model, and reaches 200% in the coarse grid model. This may occur due to a difference in size of the well blocks and the adjacent cells. In the simulation, the flow from the outlet face of the well block to the inlet faces of the adjacent cells as well as the flux between the coarsened grid cells has to be maintained at the specified rate. As a result, the pressure difference between the well blocks and the adjacent cells must be higher than the pressure difference between the inter-well coarsened grid blocks because the flow area is much smaller. In normal practice, this problem should not happen if the size of well blocks and inter-well blocks are similar, and proper near-well region upscaling is performed. In this study, the transmissibilities of the outlet faces of the injector and the inlet faces of the producer in the coarse-grid models were modified to correct the abnormal pressure drop. The correction can also be done by using nine-point scheme in Eclipse to include diagonal transmissibility values to the grid as non-neighbour connections in the areal (x-y) direction. This allows the fluid to flow in the directions not aligned with the principal directions of the grid. However, the simulation will take a longer time to run.

Vertical cross-section model

The upscaled 2D vertical cross-section models show a similar trend in oil recovery prediction to the 1D simulation result. The oil recovery predicted from the PVW pseudos is as good as the result from the 10-grid model, and reasonably matches the fine-grid solution when the pseudo-salinity thresholds are applied (Fig.20). The B-L approximated pseudos give better oil recovery at early and intermediate times than the original coarse-grid model, and give a good match in the ultimate recovery to the 10-grid model when the pseudo-salinity is applied. The water breakthrough time in the upscaled models are improved significantly although the maximum water cut is underestimated and high water cut at intermediate times is observed as shown in Fig.21. This can be further improved by using the pseudo-salinity thresholds. However, the pseudo-salinity thresholds alone cannot give an accurate prediction of water breakthrough time as seen in the 1D and 2D quarter 5-spot pattern models.

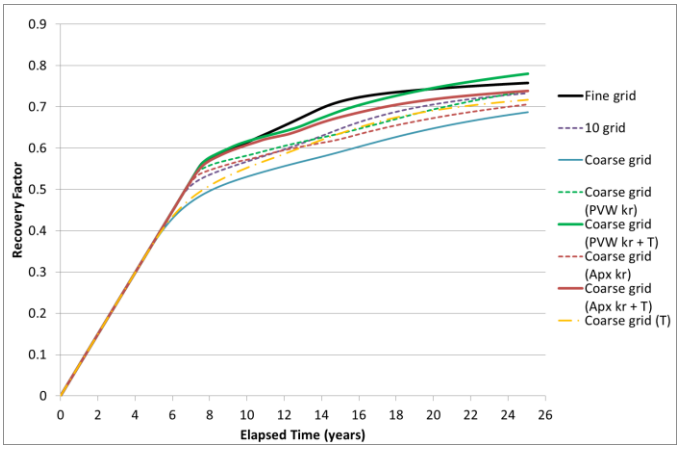

Fig.20 Effect of pseudo-k_r and salinity thresholds on oil recovery in 2D vertical cross-section models

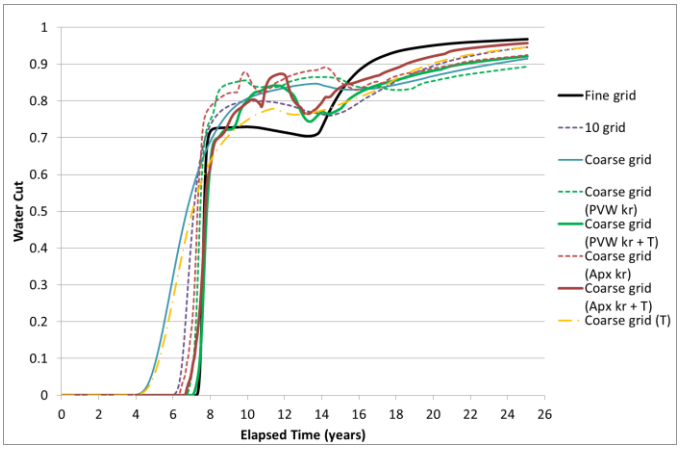

Fig.21 Effect of pseudo-k_r and salinity thresholds on water cut in 2D vertical cross-section models

The differential pressures between the injector and the producer in the 2D vertical cross-section models with different grid sizes do not significantly vary. In general, the trends are similar to the results of the 1D simulations but the pressure drops are lower because of lower reservoir flow rate. The use of pseudo-relative permeabilities still results in a decrease in the pressure drop while the pseudo-salinity thresholds cause the pressure drop to increase slightly. The characteristic of salt production rate in the vertical cross-section models throughout the field life is similar to that of the 1D models.

2D Simulation for Heterogeneous System

The PVW pseudo-relative permeability is proved to be more effective in reproducing the fine-grid oil and water production on the coarse-grid model than the B-L approximated pseudos as shown in Fig.22 and 23. It gives better overall oil recovery prediction and improves the water breakthrough time although some fluctuation in the water cut at intermediate and late times is observed whereas the B-L approximated pseudos results in more than one-year delay in the water breakthrough. The effectiveness of pseudo-salinity thresholds in complement to the pseudo-relative permeability for the layered model becomes more complicated as the simulation results of the coarse-grid models using several sets of pseudo thresholds vary significantly. T_l and T_{avg} produce similar results in both oil recovery and water cut to the coarse-grid model using only the pseudo-relative permeability. In contrast, the predictions made by T_h are very poor since it gives very optimistic oil recovery and a delayed water breakthrough. T_{apx} gives the correct water breakthrough time as well as the maximum water cut but the oil recovery is still overestimated. In terms of the salt production rate, Fig.24 shows none of the upscaled models can reproduce the fine-grid maximum salt production rate and time accurately. The result from the model using T_{apx} is probably the most accurate as it shows the correct start of salt production and a reasonable maximum rate. The pressure drops between the wells in the upscaled models are observed, and the results are consistent to the 1D and 2D homogeneous solutions in that the pseudos especially the PVW pseudos cause a decrease in pressure drop due to higher value of the oil relative permeability at low S_w.

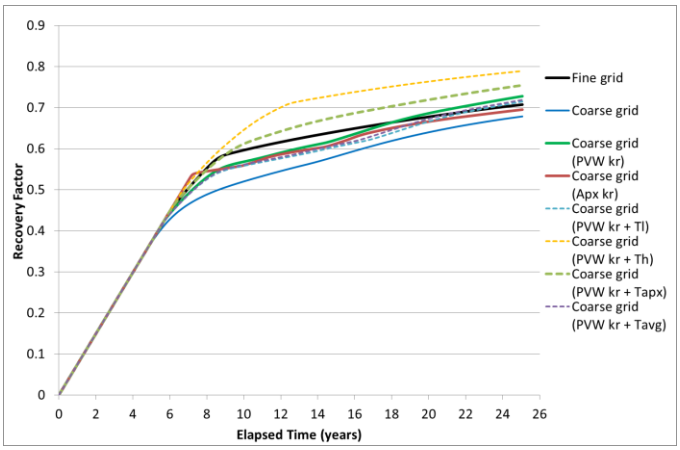

Fig.22 Effect of pseudo-k_r and salinity thresholds on oil recovery in 2D homogenised-grid models

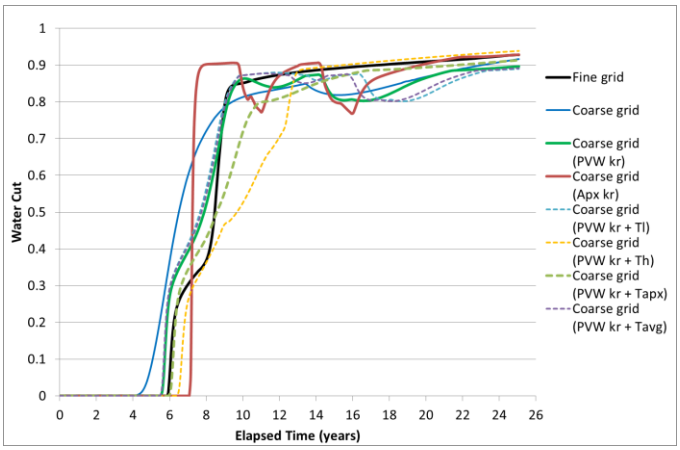

Fig.23 Effect of pseudo-k_r and salinity thresholds on water cut in 2D homogenised-grid models

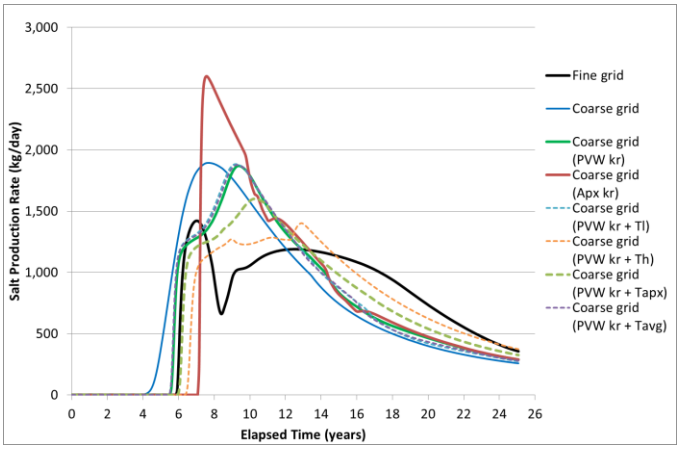

Fig.24 Effect of pseudo-k_r and salinity thresholds on salt production in 2D homogenised-grid models

3D Simulation for Heterogeneous System

From Fig.25, The oil recoveries predicted by the upscaled models using the PVW and B-L approximated pseudos are not significantly different at the late times. The difference at intermediate times is a result of a severe delay in water breakthrough predicted by the B-L approximated pseudos (Fig.26). Meanwhile, the PVW pseudos produce the correct water breakthrough time although the maximum water cut is delayed. However, in this 3D simulation, the water breakthrough time in the fine-grid model is similar to that of the coarse-grid model even when the pseudo-relative permeability is not applied. This may be because there is early breakthrough in the fine-grid model due to flow in the high permeability layer which coincidentally matches the early water breakthrough caused by numerical dispersion in the coarse grid model. The results would probably be different if the high permeability layer was thinner or the coarse grid size was changed. The effect of the pseudo-salinity thresholds on 3D flow is consistent with that seen in the 2D results that the pseudo-salinity thresholds estimated from high permeability layer (T_h) do not properly capture the low salinity effect. T_l and T_{avg} do not improve substantially the match in oil recovery from the upscaled model using only the pseudo-relative permeability. T_{apx} contributes to an overestimated oil recovery and small delay in water breakthrough although it helps improve the fluctuation in water production at the late time. The salt production graph from the 3D models in Fig.27 illustrates the same trend as in the 2D models in that the salt production rate is generally overestimated. The delay in salt production, which corresponds to the delayed water production, is observed in the upscaled model with B-L approximated pseudos. In addition, the high pressure drop problem experienced in the 2D coarse-grid quarter 5-spot pattern model is also found in the 3D coarse-grid model. The reason is the well blocks are not upscaled so the differential pressures between the well blocks to adjacent blocks at the boundary, which have smaller flow area than the inter-well coarsened grid blocks, must be increased to maintain the constant flow rate. This, therefore, affects the total pressure drop between the injection and the production well blocks.

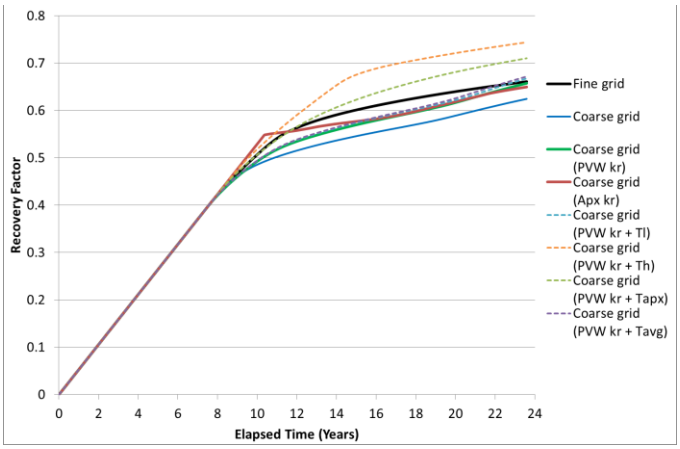

Fig.25 Effect of pseudo-k_r and salinity thresholds on oil recovery in 3D homogenised-grid models

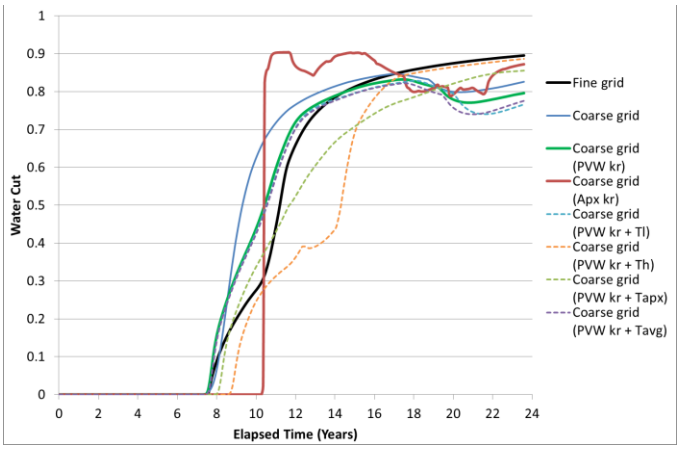

Fig.26 Effect of pseudo-k_r and salinity thresholds on water cut in 3D homogenised-grid models

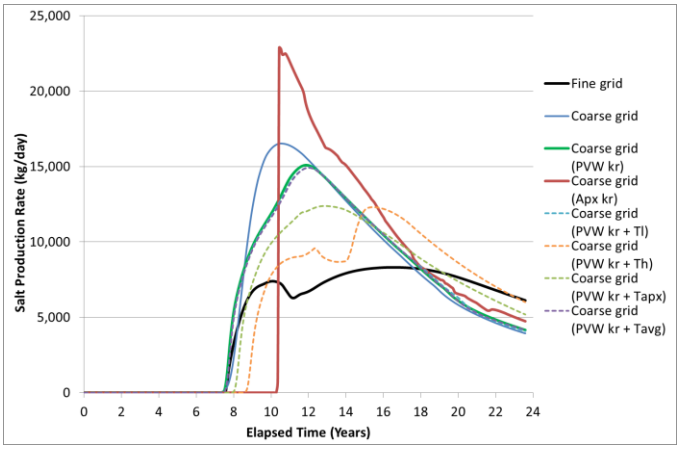

Fig.27 Effect of pseudo-k_r and salinity thresholds on salt production in 3D homogenised-grid models

Discussion

This study demonstrates the performance of using different pseudoisation techniques to compensate numerical dispersion in low salinity waterflooding upscaling in one-dimensional and multidimensional flow. In general, the simulation results show that the pseudo-relative permeability calculated by the PVW method can reproduce the fine-grid solution on the coarse-grid model more effectively than the pseudos estimated by the B-L approximation method considering mainly the oil recovery and the water breakthrough. This is because the calculation of the latter is based on the assumption of 1D linear flow whereas the PVW method uses the fine-grid simulation results to calculate the pseudo-relative permeability. Thus, the B-L approximated pseudos may not sufficiently be able to reproduce the actual behaviour in 2D and 3D, which are the combination of the flows in x, y and z-direction. Nevertheless, using the B-L approximated pseudos together with proper pseudo-salinity thresholds can reproduce the fine-grid result satisfactorily for small levels of heterogeneity while numerous sets of dynamic pseudo-relative permeabilities are required to obtain more accurate result, which are sometimes impractical. Limiting the number of coarse-grid rock types can help reducing the amount of sets of pseudos and the simulation time required (Barker and Thibeau, 1997). Also the B-L approximated pseudos can be generated off-line in a pre-processing step whilst the PVW pseudos require a fine grid simulation which, by definition, may not be possible or may be very time-consuming. More importantly, the choice of fine-grid model to be used in pseudo generation should sufficiently represent the heterogeneities in the reservoir (Muggeridge, 1991).

The modification of salinity thresholds has also been shown to be an effective pseudoisation technique for low salinity waterflooding. However, the pseudo-salinity thresholds should be carefully estimated especially in the multidimensional flow. In this study, the salt concentration profile of the fine-grid and the coarse-grid model were compared at a specific time. In the 2D vertical cross-sectional model and the 3D model, the salt concentration profiles show that the effect of numerical dispersion on the salt flow and the thresholds at which the low salinity effect appears behave differently to some degree at different depths. It is also likely that the profile varies with time and, therefore, it may be necessary to use time-dependent salinity thresholds in upscaling models. In addition, pseudo-relative permeability affects the fluid as well as salt flow behaviour. Consequently, suitable pseudo-salinity thresholds should be obtained from the salt concentration profile from the correct coarse-grid model so the final coarse-grid result can match the fine-grid result precisely. One reason why some matches between the coarse and fine grid are not precise can possibly be because the pseudo-salinity thresholds are all determined from the original coarse-grid model without upscaling.

The performance of dynamic pseudo-relative permeabilities in compensating for numerical dispersion in heterogeneous reservoir models still needs further studies on other types of heterogeneity. In this study, the results estimated by the PVW pseudos alone from the 2D and 3D homogenised-grid models show reasonable matches in the oil recovery and water breakthrough between the fine-grid and the coarse-grid model although the maximum water cut is delayed. Thus, it can be concluded that the effect of pseudo-salinity thresholds in the layered model seems to be smaller than in homogeneous or less heterogeneous systems. The reason is possibly that the low salinity effect aims to improve the oil recovery in the pore spaces where the injected low salinity water contacts. In the layered reservoir, the injected water tends to flow in the high permeability layer. As a result, most parts of the reservoir, which are less permeable, become less contacted with the low salinity water. The change in microscopic displacement efficiency due to the low salinity effect is, therefore, insubstantial compared to the macroscopic sweep efficiency. It may be acceptable to neglect the use of pseudo-salinity thresholds in this kind of heterogeneity as the estimation of appropriate pseudo thresholds can be exhaustive. However, the simulation results of the 2D and 3D homogenised-grid models indicate poor matches in salt production profiles i.e., they are overestimated. This may have an effect on the facility design in that the water treatment facilities might be overdesigned. In addition, the pressure problem, which is observed in the upscaled models caused by the use of pseudos and different grid sizes, should be considered carefully in full-field simulation. This can mislead the reservoir engineers who are responsible for pressure monitoring.

The effect of the low salinity function used in the simulation on the coarse grid model produces unusual behaviour in the profile of water production after the water breakthrough especially when pseudo-relative permeabilities are used. As the connate water bank moves through the grid cell, the water saturation of the grid cell is almost constant at S_{wcf} while the salt concentration decreases. Once the salt concentration reduces to the upper salinity threshold, the oil and water relative permeability is modified by the salinity-weighting factor. At S_{wcf}, the low salinity k_{rw} is truncated so the calculated value of k_{rw} decreases significantly according to Eq.1. This results in a decrease in the water flow rate as well as an increase in the oil flow rate, which affects the flow within the grid cell and the adjacent cells. For example, the 1D coarse-grid model with the B-L approximated pseudos (Fig.15) shows 2 sharp drops in water cut after the water breakthrough. High water cut at the breakthrough probably occurs because S_{wcf} in the upscaled model is higher than the fine grid model, and so as the k_{rw} at S_{wcf}. The water production rate is, therefore, higher. Thus, the use of pseudo-relative permeabilities in combination with similar salinity-dependent function used in this study for predicting water production requires further investigation.

Conclusions and Recommendations for Further Work

This study shows that numerical dispersion in coarse-grid models of low salinity waterflooding can be reduced effectively by using pseudo-relative permeabilities and modified salinity thresholds. The performance of two types of pseudos combined with pseudo thresholds were evaluated by comparing the reproduction of fine-grid oil recovery and water breakthrough on the coarse-grid models. From the analysis results, the following conclusion can be drawn:

1. PVW pseudo-relative permeability can be used to compensate for numerical dispersion in coarse-grid low salinity waterflood models more effectively than the Buckley-Leverett theory-based approximate pseudos. It allows equivalent reproduction of oil recovery and water breakthrough to 10-grid solutions in homogeneous systems. Using pseudo-relative permeabilities in combination with modified salinity-thresholds helps to improve the matches between fine-grid and coarse grid solutions.
2. Using analytical pseudos with proper pseudo-salinity thresholds, which are more manageable, can be considered as it can reproduce the fine-grid results reasonably well for homogeneous reservoirs or a reservoir with small levels of heterogeneity. To obtain more accurate results, a large number of sets of dynamic pseudo-relative permeabilities are typically required, which is sometimes impractical.
3. The influence of pseudo-salinity thresholds on low salinity waterflood results in highly heterogeneous reservoirs such as thin, high permeability layer model investigated in this study seems to be less significant. Pseudo-relative permeabilities alone can approximate the fine-grid behaviour on coarse-grid models satisfactorily.
4. Estimation of pseudo salinity-dependent thresholds for homogenised-grid model of heterogeneous reservoirs by comparing the salinity profiles could be very time-consuming because salt concentration distributions are not uniform.

To extend the knowledge from this study to real industry applications, further investigation on the performance of pseudo-relative permeabilities and pseudo salinity thresholds in other types of heterogeneities and real field models are suggested. In addition, further studies into developing the software that can generate salinity-dependent pseudo-relative permeability for low salinity waterflooding, and the software that can fully utilize directional relative permeabilities for multidimensional simulations could be beneficial.

Nomenclature

F_1 = salinity-dependent weighting factor
k = absolute permeability
k_r = relative permeability
S = saturation
T = pseudo-salinity thresholds
T_h = pseudo-salinity thresholds determined from high permeability layer
T_l = pseudo-salinity thresholds determined from low permeability layer
T_{apx} = pseudo-salinity thresholds approximated from both high and low permeability layers
T_{avg} = pseudo-salinity thresholds determined from average salinity distribution

Subscripts

c = connate
f = shock-front
h = high salinity
l = low salinity
o = oil
w = water

Superscripts

H = high salinity
L = low salinity

References

Barker, J.W., Dupouy, P.: "An Analysis of Dynamic Pseudo- Relative Permeability Methods for Oil-Water Flows," presented at the 5th European Conference on the Mathematics of Oil Recovery, Leoben, Austria, Sept. 2-6, 1996, and *Petroleum Geosciences* (November 1999) **4**, 385.

Barker, J.W., Thibeau, S.: "A Critical Review of the Use of Pseudorelative Permeabilities for Upscaling," paper SPE 35491 presented at the 1996 European 3D Reservoir Modelling Conference, Stavanger, 16-19 April, and *SPE Reservoir Engineering* (May 1997) **12(2)**, 138.

Christie, M.A., Blunt, M.J.: "Tenth SPE Comparative Solution Project: A Comparison of Upscaling Techniques," *SPE Reservoir Evaluation and Engineering* (August 2001) **4(4)**, 308.

Ding, Y., Renard, G.: "A New Representation of Wells in Numerical Reservoir Simulation," *SPE Reservoir Engineering* (May 1994) **9(2)**, 140.

ECLIPSE Technical Description, 2010.1 Release, Schlumberger (2010)

ECLIPSE Reference Manual, 2010.1 Release, Schlumberger (2010)

Jerauld, G.R., Lin, C.Y., Webb, K.J., Seccombe, J.C.: "Modeling Low-Salinity Waterflooding," paper SPE 102239 presented at the 2006 SPE Annual Technical Conference and Exhibition, San Antonio, Texas, Sept. 24-27, 2006.

Kyte, J.R. and Berry, D.W.: "New Pseudofunctions To Control Numerical Dispersion," *SPE Journal* (August 1975) **15(4)**, 269.

Lager, A., Webb, K. J., Black, C. J. J., Singleton, M., Sorbie, K. S.: "Low Salinity Oil Recovery: An Experimental Investigation," paper SCA2006-36 presented at the International Symposium of the Society of Core Analysts, Trondheim, Norway, Sept. 12-16, 2006.

Mahadevan, J., Lake, L.W., John, R.T.: "Estimation of True Dispersivity in Field Scale Permeable Media**,**" paper SPE 75247 presented at the SPE/DOE Improved Oil Recovery Symposium, Tulsa, Oklahoma, U.S.A, Apr. 13-17, 2002

McGuire, P.L., Chatam, J.R., Paskvan, F.K., Sommer, D.M. and Carini, F.H.: "Low Salinity Oil Recovery: An Exciting New EOR Opportunity for Alaska's North Slope," paper SPE 93903 presented at the 2005 SPE Western Regional Meeting, Irvine, CA, U.S.A., 30 Mar. 30 – Apr. 1, 2005.

Muggeridge, A.H.: "Generation of Effective Relative Permeabilities from Detailed Simulation of Flow in Heterogeneous Porous Media," *Reservoir Characterization II*, L.W. Lake, H.B. Carroll, and T.C. Wes- son (eds.), Academic Press, San Diego, California (1991) 197.

PSEUDO Reference Manual, 94A Release. Intera Information Technologies Ltd (1994)

Russel, R.G., Morgan, F., Muskat, M.: "Some Experiments on the Mobility of Interstitial Waters," *Transactions of the AIME* (December 1947) **170(1)**, 51.

Salter, S. J., and Mohanty, K.K.: "Multiphase Flow in Porous Media: I. Macroscopic Observations and Modeling," paper SPE 11017 presented at the 57th Annual Fall Technical Conference and Exhibition of the Society of Petroleum Engineers of AIME, New Orleans, LA, Sept. 26-29, 1982.

Tang, G.Q., Morrow, N.R.: "Salinity, Temperature, Oil Composition, and Oil Recovery by Waterflooding," *SPE Reservoir Engineering* (November 1997) **12(4)**, 269.

Webb, K.J., Black, C.J.J., Edmonds, I.J.: "Low Salinity Oil Recovery - The Role of Reservoir Condition Corefloods," presented at the 13th European Symposium on Improved Oil Recovery, Budapest, Hungary, Apr. 25-27, 2005.

Yildiz, H.O., Morrow, N.R.: "Effect of composition on recovery of Moutray crude oil by waterflooding," *Journal of Petroleum Science & Engineering* (1996) **14**. 159.

Appendix A - Critical Literature Review

MILESTONES IN UPSCALING LOW SALINITY WATERFLOODING
TABLE OF CONTENT

SPE Paper n°	Year	Title	Authors	Contribution
Reservoir Characterization II	1991	"Generation of Effective Relative Permeabilities from Detailed Simulation of Flow in Heterogeneous Porous Media"	Muggeridge, A.H.	Demonstrate the importance of defining reservoir volume elements containing the appropriate permeability distribution for pseudo function generation
Journal of Petroleum Science & Engineering Vol.14	1996	Effect of composition on recovery of Moutray crude oil by waterflooding	Yildiz, H.O., and Morrow, N.R.	First to show that oil recovery can be improved by changing injected brine composition
SPE Reservoir Engineering, Vol.12, No.4	1997	Salinity, Temperature, Oil Composition, and Oil Recovery by Waterflooding	Tang, G.Q., and Morrow, N.R.	First to show that oil recovery can be increased by lowering the salinity of either connate brine or injected brine
Petroleum Geoscience Vol.5	1999	"An Analysis of Dynamic Pseudo-Relative Permeability Methods for Oil-Water Flows"	Barker, J.W., and Dupouy, P.	Provide a summary of properties and limitations of widely used dynamic pseudoisation methods for relative permeability
SPE Reservoir Engineering, Vol.12, No.2	1997	"A Critical Review of the Use of Pseudorelative Permeabilities for Upscaling"	Barker, J.W., and Thibeau, S.	Introduce common practical difficulties in using dynamic pseudorelative permeabilities for upscaling
SPE Reservoir Evaluation and Engineering, Vol.4, No.4	2001	"Tenth SPE Comparative Solution Project: A Comparison of Upscaling Techniques"	Christie, M.A., and Blunt, M.J.	Demonstrate that upscaling approaches which only the absolute permeability is used, and excessive grid coarsening can give a significant discrepancy between coarse-grid and fine-grid simulation results.
102239	2006	"Modeling Low-Salinity Waterflooding"	Jerauld, G.R., Lin, C.Y., Webb, K.J., and Seccombe, J.C.	First to use salinity-dependent oil/water relative permeability to model low-salinity waterflooding, and use pseudoisation by changing salinity-dependent thresholds and the curve shapes to match the results from a coarse model to a fine model.

Reservoir Characterization II, 197-225 (1991)

Generation of Effective Relative Permeabilities from Detailed Simulation of Flow in Heterogeneous Porous Media

Authors: Muggeridge, A.H.

Contribution to the understanding of upscaling low salinity waterflooding:

Show that the effective relative permeability can accurately represent the fluid flow through the reservoir if the reservoir section used to generate it appropriately captures the permeability distribution

Objective of the paper:

To study how well effective permeabilities represent the average properties of fluid flow through the reservoirs with different permeability distributions.

Methodology used:

1. Use high-resolution simulation described by Christie (1989) to generate effective permeabilities for the representative sections of three waterflood models with different permeability distributions and correlation lengths, namely an uncorrelated, log-normal permeability distribution, a sandbody distribution containing different five types of sand, and hypothetical channel sand made up with two rock types.
2. For each model, a 2D heterogeneous, fine-grid model was reduced to 1D homogeneous models either a single grid block or a row of four grid blocks. The effective absolute permeabilities and effective relative permeabilities of new grid blocks were generated using the pressure-solver method by Begg et al. (1987), and the methods of Jones and Roszelle (1978), respectively.
3. The results of the flow simulations from both single-grid block models and four-grid block model were compared with those from the original fine-grid models to determine the accuracy of the effective properties.

Conclusion reached:

1. Some deviation in the shape of effective relative permeabilities and oil recovery curves can be expected for more correlated permeability distributions such as a sand channel model.
2. The selected volume of the reservoir used to produce the effective properties must contain a representative section of the permeability distribution where the flow will be modelled. Otherwise, the generated properties might not reproduce find-grid solutions on coarse-grid models.

Comments:

This study provides a basis on grid selection, which can be generally applied to upscaling of a fine-grid simulation to obtain pseudo functions that accurately represent the fine-grid results.

Journal of Petroleum Science & Engineering 14, 159-168 (1996)

Effect of composition on recovery of Moutray crude oil by waterflooding

Authors: Yildiz, H.O., and Morrow, N.R.

Contribution to the understanding of upscaling low salinity waterflooding:

Prove that injected brine composition affects oil recovery by waterflooding and the higher waterflood recovery can be achieved by making the system less water-wet.

Objective of the paper:

1. To confirm the effect of brine composition on oil recovery by waterflooding in different crude oil/brine/rock systems
2. To determine the effect of having different initial and injected brines, and the importance of a soaking period before changing the composition of injected brine.

Methodology used:

1. Standard waterfloods and imbibition tests, which used the same initial and injected brines, were performed on core samples from Berea Sandstone. The samples were treated to achieve mixed-wet states and two types of brines were used in the experiments.
2. Mixed-brine tests were performed by varying initial brines, first and second injected brines. 10-day soaking period was allowed before changing the injected brine composition.
3. The effect of crude oil composition and aging conditions on recovery was presented by comparison of the standard waterflood test results which performed on a different crude oil and aging temperature.

Conclusion reached:

1. The less water-wet system gives the higher oil recovery by standard waterfloods.
2. Changing the brine composition can possibly improve oil recovery when it is compared to standard waterfloods. This is probably because of changes in crude oil/rock/brine interactions. However, the effect of brine composition is strictly specific to the system conditions.

Comments:

As the impact of brine composition is specific to the conditions of the tests, the relative importance of crude oil, rock and brine on the factors that control recovery including wettability should be further investigated.

SPE Reservoir Engineering, Vol.12, No.4, 269-276 (Nov 1997)

Salinity, Temperature, Oil Composition, and Oil Recovery by Waterflooding

Authors: Tang, G.Q., and Morrow, N.R.

Contribution to the understanding of upscaling low salinity waterflooding:

Show that lowering connate or injected brine salinity can improved oil recovery by waterflooding

Objective of the paper:

To investigate the effect of brine and oil compositions, and aging and displacement temperatures on wettability and oil recovery by waterflooding and spontaneous imbibition

Methodology used:

Perform spontaneous imbibition and waterflood tests on the core samples of Berea sandstone by varying the following parameters.

1. Salinity of connate brines and/or injected brines by changing brine concentration
2. Imbibition and waterflood temperatures by increasing the temperature from 22 to 75°C for different pairs of crude oils and brines
3. Crude oil composition by removing and adding light components (hexane, heptane, octane)
4. Aging time

Oil recovery by spontaneous imbibition and waterflooding were determined and compared. The effect of aging temperature was compared to the results from other studies.

Conclusion reached:

1. Oil recovery by spontaneous imbibition and waterflooding increases as salinity decreases.
2. An increase in displacement temperature can result in a wettability change toward water wet and an increase in oil recovery.
3. Removal of light components resulted in a decrease in water wetness and oil recovery while addition of alkanes reduced water wetness, and increased oil recovery.

Comments:

From the conclusion of this study, the trends between wettability and oil recovery for the changes in various variables is not necessarily consistent. However, wettability should be considered in waterflood study because oil recovery can be improved by changing the reservoir wettability.

Petroleum Geoscience, Vol.5, 385-394 (Nov 1999)

An Analysis of Dynamic Pseudo- Relative Permeability Methods for Oil-Water Flows

Authors: Barker, J.W., and Dupouy, P.

Contribution to the understanding of upscaling low salinity waterflooding:

Provide an analysis of properties and limitations of dynamic pseudoisation methods for relative permeability

Objective of the paper:

To analyse the properties of six widely used dynamic pseudorelative permeabilities by considering the displacement of oil by water.

Methodology used:

The simplified Stone's example (1991) of a dipping vertical cross-section with two layers with different permeabilities and no communication is used to compare the properties of the six methods, namely Kyte & Berry, PVW, Stone's, Quasi-Steady State, Weighted Relative Permeability and Total Mobility.

Conclusion reached:

1. The Kyte & Berry and PVW methods can reproduce a fine-grid result on a coarse grid but negative or infinite value of pseudorelative permeability is possible. Position-dependent effective pseudocapillary pressure is also required for Kyte & Berry method
2. Reproduction of the fine-grid solution cannot be guaranteed by using the Total Mobility, Stone's, Quasi-Steady State or Weighted Relative Permeability methods. However, the Total Mobility methods can be reliable in simple cases.

Comments:

There is no ideal dynamic pseudorelative permeability method for upscaling. Different methods should be evaluated to obtain the most appropriate solution for a particular case.

SPE Reservoir Engineering, Vol.12, No.2, 138-143 (May 1997)

A Critical Review of the Use of Pseudorelative Permeabilities for Upscaling

Authors: Barker, J.W., and Thibeau, S.

Contribution to the understanding of upscaling low salinity waterflooding:

Introduce severe difficulties in using dynamic pseudorelative permeabilities for upscaling including grouping coarse grid blocks so the number of set of pseudos can be minimised.

Objective of the paper:

To summarize the properties and limitation of various dynamic pseudorelative permeability methods and to address practical difficulties of using these methods to reproduce the results of fine grid simulations on coarse grid models.

Methodology used:

Summarized pros and cons of different dynamic pseudorelative permeability methods and discussed practical difficulties that prevent these methods to be used in upscaling reliably. Also, a practical approach to upscaling using pseudos is suggested.

Conclusion reached:

1. Because dynamic pseudos depends on well rates and position, and they need to be regenerated from fine-grid simulation, a large number of sets of pseudos can be expected leading and so the computer time required. Thus, choice of coarse-grid rock types should be limited and choices of fine-grid models should sufficiently represent reservoir heterogeneities.
2. The use of pseudorelative permeabilities in upscaling can be reliable if capillary or gravity equilibrium can be assumed at coarse-grid scale.

Comments:

This paper provides useful guidelines in upscaling especially for full field simulations, which can be an extended study of this project.

SPE Reservoir Evaluation and Engineering, Vol.4, No.4, 308-317 (Aug 2001)

Tenth SPE Comparative Solution Project: A Comparison of Upscaling Techniques

Authors: Christie, M.A., and Blunt, M.J.

Contribution to the understanding of upscaling low salinity waterflooding:

Demonstrate that upscaling approaches which only the absolute permeability is used, and excessive grid coarsening can give a significant discrepancy between coarse-grid and fine-grid simulation results.

Objective of the paper:

To compare the results of the 10th SPE Comparative Solution Project on Upscaling, which different upgridding and upscaling techniques were used for two defined models by 9 participants.

Methodology used:

1. Two models were used in this project. The first model was a simple 2D vertical cross-section of immiscible gas injection without connate water. The second model was a 3D waterflood with 1.1-million-cell geostatistical model.
2. The fine-grid solutions were produced by different parallel reservoir simulators, or streamline-based reservoir flow simulators.
3. The upscaled solutions were computed in two approaches. The first approach is to use the information from fine-scale simulation to determine relative permeabilities for a coarse-grid model. The other approach is to use a single-phase upscaling with or without flow-based upgridding. Various upgridding and upscaling methods were used.

Conclusion reached:

1. Single-phase upscaling and appropriate local grid refinement can give a good match between fine-grid and coarse-grid results for Model 1.
2. Some discrepancies can be observed in the coarse-grid solutions when only absolute permeability upscaling and excessive grid coarsening were applied. Regression-based pseudoisation of relative permeability can give good agreement. However, different upscaling methods gave variation in the results to some extent.
3. In this exercise, flow-based upscaling with no flow boundary condition was the best single-phase method while linear-pressure boundary condition has proved to give an improvement in upscaling for other geological models.

Comments:

Relative permeability upscaling is important especially for highly heterogeneous system. However, different upscaling methods need to be evaluated for each geological model as there is no ideal technique.

SPE 102239 (2006)

Modeling Low-Salinity Waterflooding

Authors: Jerauld, G.R., Lin, C.Y., Webb, K.J., and Seccombe, J.C.

Contribution to the understanding of upscaling low salinity waterflooding:

Develop the 1D model which represents low-salinity waterflooding using salinity-dependent oil/water relative permeability functions, and apply pseudoisation by changing relative permeability curves in a coarse grid simulation to capture physical dispersion in a fine grid model.

Objective of the paper:

To describe the model of low salinity waterflooding, which can represent corefloods, SWCTTs, and field scale simulations for oil recovery estimation.

Methodology used:

Use conventional waterflood modelling in BP's version of VIP^{TM} by adding low salinity model consisting of salt, salinity-dependent relative permeability and capillary pressure, inaccessible portions of the connate water, hysteresis between imbibition and secondary drainage relative permeability, and a dispersion model within the water phase.

Conclusion reached:

1. This model of salinity-dependent relative permeability and capillary pressure can be used to describe the secondary and tertiary low salinity waterflooding in 1D.
2. Numerical dispersion can represent appropriately physical dispersion given a number of grid blocks of 10-25 between an injector and a producer.
3. Modifying salinity dependence thresholds and relative permeability curves on coarse grid simulations can be applied to give a reasonable match to fine grid results in 1D.

Comments:

1. Pseudoisation of relative permeability for upscaling in 1D was proved to be effective. However, evaluation on multidimensional simulation is required.
2. The suitable number of grid blocks between a producer and an injector to represent correct levels of dispersion for different heterogeneity of reservoirs needs to be studied.

Appendix B – Rock Relative Permeability Data

The following oil and water relative permeabilities for high and low salinity systems were taken from the Eclipse low salinity water injection example data file. They are used for all fine-grid low salinity waterflood simulations in this study.

Table B1 – High salinity oil and water relative permeabilities

S_w	k_{rw}	k_{ro}	P_c
0.2	0	1	0
0.255	0.005	0.729	0
0.31	0.02	0.512	0
0.365	0.045	0.343	0
0.42	0.08	0.216	0
0.475	0.125	0.125	0
0.53	0.18	0.064	0
0.585	0.245	0.027	0
0.64	0.32	0.008	0
0.695	0.405	0.001	0
0.75	0.5	0	0
1	1	0	0

Table B2 – Low salinity oil and water relative permeabilities

S_w	k_{rw}	k_{ro}	P_c
0.15	0	1	0
0.225	0.004	0.729	0
0.3	0.014	0.512	0
0.375	0.032	0.343	0
0.45	0.056	0.216	0
0.525	0.088	0.125	0
0.6	0.126	0.064	0
0.675	0.172	0.027	0
0.75	0.224	0.008	0
0.825	0.284	0.001	0
0.9	0.35	0	0
1	1	0	0

Appendix C – Upscaling of Two-Phase Relative Permeabilities to Compensate for Numerical Dispersion by Ann H. Muggeridge (November 2007, Updated July 2013)

Abstract
This note uses Buckley-Leverett theory to derive upscaled, two-phase relative permeabilities for use in coarse grid numerical simulation. These pseudo relative permeabilities compensate for numerical dispersion. The current derivation assumes linear flow and neglects gravity. The derivation also shows the importance of appropriate discretization of relative permeability curves for input into numerical simulation.

In contrast to previous methods this derivation shows that reasonable results can be obtained if only 2 pairs of pseudo curves are provided to the simulator: 1 pair of curves for the injection well block and the second pair of curves to be used elsewhere. The method is tested successfully on simple 1D models.

Introduction
Relative permeabilities, measured from displacements through rock cores in the laboratory (often referred to as 'rock curves'), are often altered before input into a simulator in order to better represent the effects of reservoir heterogeneity on flow and compensate for numerical dispersion in the field scale model. There is a large literature on this activity, which will not be referred to here. Instead the interested reader is referred to the review papers by Barker and Thibeau (1997), Barker and Dupouy (1996) and Christie (1996).

Most two phase upscaling methods attempt to represent the effects of heterogeneity on flow and compensate for numerical dispersion simultaneously. However in this note we shall follow the approach advocated by Muggeridge (1991) and discussed in more detail by Mahani and Muggeridge (2005) in which upscaling is divided into two steps, the first homogenizing the coarse grid cell and the second compensating for numerical dispersion. In particular we shall examine how best to compensate for numerical dispersion in coarse grid reservoir simulation. As a result we shall assume homogeneous fine grid and coarse grid simulation models.

Buckley-Leverett Theory
We shall assume that the displacement of oil by water is described by the two-phase extension to Darcy's Law:

$$q_w = -kA\frac{k_{rw}}{\mu_w}\frac{\partial p}{\partial x}$$
$$q_o = -kA\frac{k_{ro}}{\mu_o}\frac{\partial p}{\partial x} \qquad (1)$$

where we have ignored the effects of gravity and capillary pressure. Here q_w is the volumetric flow rate of water, q_o is the volumetric flow rate of oil, k is the permeability, A is the cross-sectional area, k_{rw} is the relative permeability to water, k_{ro} is the relative permeability to oil, μ_w is the water viscosity, μ_o is the oil viscosity and p is pressure.
We can express the conservation of water in 1D as:

$$\frac{\partial s_w}{\partial t} + \frac{q_t}{A\phi}\frac{\mathrm{d}\, f_w}{\mathrm{d}\, s_w}\frac{\partial s_w}{\partial x} = 0 \qquad (2)$$

where s_w is the water saturation, q_t is the total flow rate $(=q_o+q_w)$, f_w is the fractional flow of water defined by

$$f_w = \frac{k_{rw}/\mu_w}{k_{rw}/\mu_w + k_{ro}/\mu_o} \qquad (3)$$

and ϕ is porosity.
Combining equations (1) and (2) we obtain the familiar Buckley-Leverett equation (Buckley and Leverett, 1942)

$$\left.\frac{\mathrm{d}\, x}{\mathrm{dt}}\right|_{s_w} = \left.\frac{q_{t_S}}{A\phi}\frac{\mathrm{d}\, f_w}{\mathrm{d}\, s_w}\right|_{s_w} \qquad (4)$$

This states that individual saturations advance through the reservoir with a characteristic velocity determined by the gradient of the fractional flow curve at that saturation. Equation (4) can be re-written in dimensionless units as

$$V_{sw} = \left.\frac{\mathrm{d}\, f_w}{\mathrm{d}\, s_w}\right|_{s_w} \tag{5}$$

In most cases the gradient of the fractional flow has an inflection i.e. the gradient increases and then decreases. This results in the formation of a discontinuous shock front in water saturation which propagates through the reservoir (figure 1). The saturation of the shock front can be determined by the Welge construction (Welge, 1952).

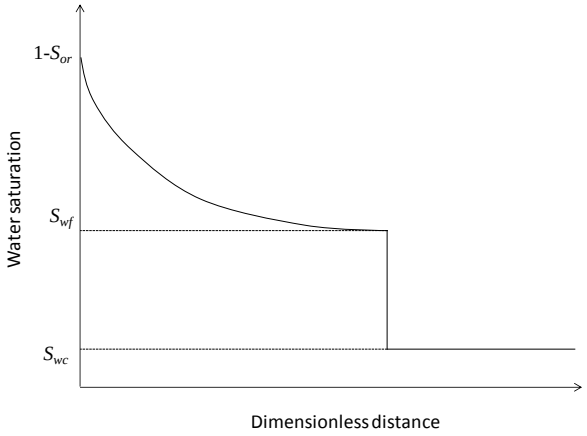

Figure 1

The Buckley-Leverett equation tells us that any chosen saturation will move through the reservoir at a velocity determined by the gradient of the fractional flow curve. The fractional flow gradient usually has an inflection which results in the formation of a shock front as shown in the above plot of water saturation versus distance.

The speed of travel of the shock front will determine water breakthrough time in a homogeneous reservoir and the height of the shock and development of the rarefaction wave behind the shock will control the subsequent water cut development with time. Thus it is important to accurately describe this saturation profile and its motion in reservoir simulation.

Calculation of Pseudo Relative Permeabilities

Most simulators use a first order, finite volume formulation to approximate the flow equations. In particular they determine the saturation dependent flow terms using upstream weighting. Using the notation shown in Figure 2, the total velocity for flow from grid block i to grid block i+1 is determined from

$$v_{i+1/2} = -k_{i+1/2}\left(\frac{k_{rw}(s_{w,i})}{\mu_w} + \frac{k_{ro}(s_{w,i})}{\mu_o}\right)\frac{(p_{i+1} - p_i)}{\Delta x} \tag{6}$$

where $i + 1/2$ is used to denote a quantity evaluated at the boundary between grid i and grid block i+1. The relative permeabilities are determined for the water saturation in the upstream grid block i. Normal first order finite difference simulators assume the water saturation is uniform within any given grid block as shown in Figure 2. Thus once water enters a grid block it is able to flow out of the opposite face of that grid block in the next time step even if in reality the water front may not yet have reached the location of the grid block outlet face (see grid block i=5 in Figure 2). This results in the simulator predicting a smeared shock front and is described as numerical dispersion. The smearing increases as the number of grid blocks decreases.

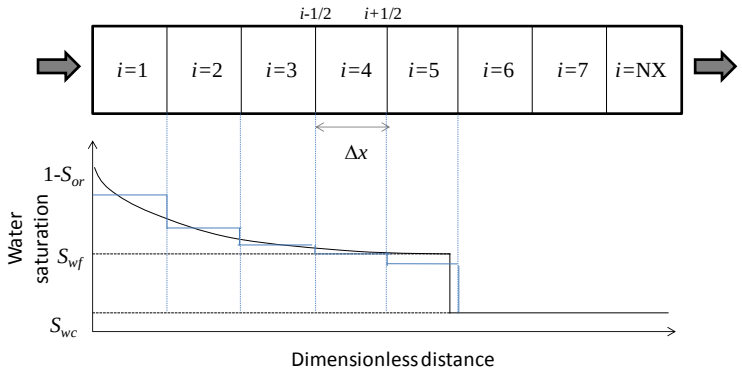

Figure 2

Cartoon showing a 1 dimensional grid used to model a waterflood. Water is injected across the left face of grid block 1 and oil and water are produced across the right hand face of grid block NX. Underneath is shown the ideal water saturation distribution as

predicted by Buckley-Leverett analysis and the pore volume weighted average water saturation in each grid block.

The relationship between number of grid blocks and numerical dispersion has been analysed by Lantz (1971). It can be seen that the finer the grid the better the approximation to the analytic saturation profile. However in many field scale simulations it is not possible to use a large enough number of grid cells between wells to minimise numerical diffusion due to memory and CPU constraints.

In this note we show that it is possible to calculate a set of pseudo relative permeabilities that, when used as input in a homogeneous coarse grid simulation, will reproduce the water saturation and pressure distributions seen in a homogeneous fine grid simulation. We shall assume that the laboratory has provided us with the measured (rock) relative permeabilities in the form of a single table containing n values of water saturation s_{wj}, k_{rwj}, k_{roj}. Normally the engineer would enter these directly into his or her fine grid simulation input data set and then use simulation to generate pseudo or upscaled relative permeabilities.

In this work we shall provide the equations for converting these rock curve tables into one or more tables of pseudo relative permeability tables each also containing n values of S_{wj}, K_{rwj}, K_{roj}. In the process we will gain an insight into how discretising relative permeability curves may affect the accuracy of flow simulation.

As note above, finite volume simulation assumes that the saturation or pressure in any grid block is the volume average of the actual saturation or pressure distribution within that grid block. Clearly for coarse grids the 1D finite difference solution will be closer to the analytical solution if relative permeability curves are tabulated as a function of average saturation within that grid block,

$$\overline{S_w} = \frac{1}{\Delta x}\int_{x_{i-1/2}}^{x_{i+1/2}} s_w \,\mathrm{dx} \tag{7}$$

where $s_w(x)$ is determined from the Buckley-Leverett equation and Δx is the length of the grid block. In addition smearing of the front will be reduced by setting the water relative permeability to zero for water saturations below the mean grid block saturation corresponding to the point when the shock front reaches the outlet face of the grid block. However if we do this we will reduce the total mobility in a given grid block and thus increase the resistance to flow. We can rewrite equation (6) as

$$v_{i+1/2} = -k_{i+1/2}\lambda_{Ti}\frac{(p_{i+1}-p_i)}{\Delta x} \tag{8}$$

where $\lambda_{T,i} = \dfrac{k_{rw}(s_{w,i})}{\mu_w} + \dfrac{k_{ro}(s_{w,i})}{\mu_o}$ is the total mobility. Setting k_{rw}=0 for water saturations less than the shock front saturation reduces this total mobility for these water saturation. To compensate for this the oil relative permeability needs to be increased. We need to ensure that pressure gradient calculated for a given interstitial velocity on the coarse grid

$$\frac{P_{i+1}-P_i}{\Delta x} = \frac{V_{i+1/2}}{k_{i+1/2}L_o(S_{w,i})} \tag{9}$$

is the same as that calculated from Darcy's law

$$\frac{\partial P}{\partial x} = \frac{v}{\Delta x k}\int_{x_{i-1/2}}^{x_{i+1/2}} \frac{\mathrm{dx}}{\lambda_T} \tag{10}$$

where the pseudo oil mobility is given by $L_o = K_{ro}/\mu_o$. Note the use of capital letters to denote upscaled quantities.

Equating equations (9) and (10) and simplifying we obtain

$$\frac{1}{L_o(\overline{S_{w,I}})} = \frac{1}{\Delta x}\int_{x_{i-1/2}}^{x_{i+1/2}} \frac{\mathrm{dx}}{\lambda_T} \tag{11}$$

Once the shock front has reached the outlet face of the grid cell then both oil and water relative permeabilities need to be adjusted so that both the coarse grid block total mobility and the coarse grid block fractional flow is the same as that obtained by volume averaging the water saturation distribution obtained by the Buckley-Leverett solution

$$\frac{1}{L_T\left(\overline{S_{w,i}}\right)} = \frac{1}{\Delta x}\int_{x_{i-1/2}}^{x_{i+1/2}} \frac{\mathrm{dx}}{\lambda_T}$$
$$F_w = \frac{L_w\left(\overline{S_{w,i}}\right)}{L_T\left(\overline{S_{w,i}}\right)} = \frac{\lambda_w\left(s_{w(i+1/2)}\right)}{\lambda_T\left(s_{w(i+1/2)}\right)} \qquad (12)$$

Close examination of the saturation distributions seen in the simulation of a 1 dimensional line drive with the injector in the first grid block and the producer in the last grid block (as shown in Figure 2) shows that there will be two types of inlet saturations for grid blocks:

1. In the injection well block the inlet saturation will always be ($1-s_{or}$)
2. In intermediate grid blocks the saturation at the inlet face will be equal to that of the outlet face of the preceding grid block.

We will calculate the pseudo relative permeabilities for each of these cases in turn using equations (11) and (12).

The first step in the pseudoization process for both grid blocks is to identify the location of the shock front saturation s_{wf} in the rock curve table. We shall assume that each relative permeability table is formed of n values as shown below:

$s_{w,1}$	$k_{rw,1}$	$k_{ro,1}$
$s_{w,2}$	$k_{rw,2}$	$k_{ro,2}$
...	...	...
$s_{w,j}$	$k_{rw,j}$	$k_{ro,j}$
...	...	...
$s_{w,n-1}$	$k_{rw,n-1}$	$k_{ro,n-1}$
$s_{w,n}$	$k_{rw,n}$	$k_{ro,n}$

We shall denote the location of any given saturation by j and the location of the shock front saturation in the table as J. This can easily be achieved either graphically using the Welge analysis or numerically. Note that this (and thus the pseudo relative permeabilities) will depend upon the water and oil viscosities as well as the relative permeabilities. Once the shock front saturation has been identified then the calculation of pseudo relative permeabilities can then be performed for the two different inlet boundary conditions as follows:

Injection well block

The first step is to calculate the dimensionless time that the water shock front reaches the outlet face of the first grid block using equation (5)

$$\tau = \frac{\left(s_{wJ} - s_{wc}\right)}{f_{wJ}} \qquad (13)$$

Thus each of the saturations greater than the shock front will have travelled a distance given by

$$x_j = \frac{\left(f_{wj} - f_{w(j+1)}\right)}{\left(s_{wj} - s_{w(j+1)}\right)}\frac{\left(s_{wJ} - s_{wc}\right)}{f_{wJ}} \qquad (14)$$

Hence we can calculate the total mobility at the time the shock front reaches the outlet face of the grid block using equation (11)

$$\frac{1}{L_{TJ}} = \frac{\left(s_{wJ} - s_{wc}\right)}{f_J}\sum_{j=J}^{j=n-1}\left[\frac{\left(f_{wj} - f_{w(j+1)}\right)}{\left(s_{wj} - s_{w(j+1)}\right)} - \frac{\left(f_{w(j+1)} - f_{w(j+2)}\right)}{\left(s_{w(j+1)} - s_{w(j+2)}\right)}\right]\frac{1}{\lambda_{Tj}} \qquad (13)$$

For $j<J$ the rock water relative permeability values k_{rwj} are replaced with $K_{rwj} = 0$ (note use of capitals to denote the pseudo values). Keeping the same saturation values in the pseudo relative permeability table for $j<J$ means that those saturation values are related to the mean saturation $\overline{S_{wf}}$ behind the shock front and the distance moved by the shock front Δx from the inlet by:-

$$s_{wj} = \frac{\Delta x}{\Delta X}\overline{S_{wf}} + \left(1 - \frac{\Delta x}{\Delta X}\right)s_{wc} \tag{15}$$

where ΔX is the length of the grid block in the direction of flow.

The pseudo oil mobility for each existing water saturation in the relative permeability when the shock front has not reached the outlet face of the grid block (i.e. when $s_{wj} < \overline{S_{wf}}$) is given

- by the saturation weighted harmonic average of the average total mobility behind the shock front and
- the oil total mobility in the absence of water (ahead of the shock front)

or mathematically as

$$\begin{aligned}\frac{1}{L_{oj}} &= \frac{\Delta x}{\Delta X}\frac{1}{L_{TJ}} + \left(1 - \frac{\Delta x}{\Delta X}\right)\frac{1}{\lambda_o(s_{wc})} \\ &= \left(\frac{s_{w,j} - s_{wc}}{\bar{S}_{wf} - s_{wc}}\right)\frac{1}{L_{TJ}} + \left(1 - \frac{s_{w,j} - s_{wc}}{\bar{S}_{wf} - s_{wc}}\right)\frac{1}{\lambda_o(s_{wc})}\end{aligned} \tag{16}$$

where s_{wc} is the connate (immobile) water saturation.

For $j \geq J$ water saturations in the table are replaced with values determined from

$$S_{wj} = s_{wj} + \frac{(1 - f_w(s_{wj}))}{df_w / ds_w\big|_{s_{wj}}} \tag{17}$$

i.e. the mean water saturation corresponding to the water saturation at the outlet face of the grid block. For the derivation of this equation see Chapter 10 of Dake (1971). For tabular rock relative permeability curves equation (17) becomes

$$S_{wj} = s_{wj} + \frac{(1 - f_{wj})(s_{wj} - s_{w(j+1)})}{(f_{wj} - f_{w(j+1)})} \tag{18}$$

Note that the choice of forward or backward difference for the fractional flow gradient will affect the shock front saturation and velocity. The backward difference used in equation (18) is consistent with water displacing oil.

The total mobility for $j \geq J$ is given by equation (13) in which the summation is changed to be from j to n rather than from J to n and the characteristic time is now the time taken for the saturation of interest to reach the outlet face of the grid block (i.e. $\frac{s_{wj} - s_{w,j+1}}{f_{wj} - f_{w,j+1}}$ The oil and water pseudo relative permeabilities can then be deduced from the total pseudo mobility and the fractional flow for the saturation at the grid block outlet by application of equation (12)

Note that this pseudoisation to compensate for numerical dispersion in the injection well block is independent of the size of the block or the number of the cells between injection and production wells.

Grid blocks without an injection well

For grid blocks not containing an injection well, the calculation of pseudo relative permeabilities is as follows:

1. set K_{rw}=0.0 (remember capitals denote a pseudo quantity) for all saturations less than the shock front saturation, s_{wf}
2. adjust the oil mobilities for $s_{wj} < s_{wf}$ to ensure the grid block total mobility matches that for two phase flow.

We shall show that in most circumstances it is unnecessary to replace the saturations with average saturations for $s_{wj} > s_{wf}$.

The mean water saturation in grid block i is obtained from the difference between the volume of water found between the injection well and the outlet of the grid block of interest and the volume of water found between the injection well and the inlet of the grid block of interest divided by the grid block volume i.e.

$$\begin{aligned}s_{wj} &= \left[i\Delta x\phi\bar{S}_{w,i+\frac{1}{2}} - (i-1)\Delta x\phi\bar{S}_{w,i-\frac{1}{2}}\right] \Big/ \phi\Delta x \\ &= i\bar{S}_{w,i+\frac{1}{2}} - (i-1)\bar{S}_{w,i-\frac{1}{2}}\end{aligned}$$

where $\overline{S_{w,i+\frac{1}{2}}}$ is the mean saturation calculated for the reservoir volume from the injection well to the outlet face of the grid

block, $\overline{S_{w,i-1/2}}$ is the mean saturation between the injection well and the inlet face of the grid block, Δx is the grid block length (uniform grid block sizes assumed) and ϕ is the porosity (again assumed uniform everywhere). This is obviously for the case after the shock front has passed through the grid block.

Using Chapter 10 of Dake we can express the mean water saturations in terms of the fractional flows and the gradient of the fractional flows as follows

$$\begin{aligned}\bar{S}_{w,i} &= s_{w,j} \\ &= i\left[s_{wO} + \frac{(1-f_w(s_{wO}))}{df_w/ds_w\big|_{s_{wO}}} \right] - (i-1)\left[s_{wI} + \frac{(1-f_w(s_{wI}))}{df_w/ds_w\big|_{s_{wI}}} \right]\end{aligned} \tag{19}$$

where s_{wI} is the point saturation value at the inlet and s_{wO} is the point saturation value at the outlet i.e. we have replaced the notation of $\left(i \pm \frac{1}{2}\right)$ with either *I* or *O* as this is quicker to write.

Rearranging equation (19) we get

$$s_{wj} = \left[s_{wI} + \frac{(1-f_w(s_{wI}))}{df_w/ds_w\big|_{s_{wI}}} \right] + i(s_{wO} - s_{wI}) + i\left[\frac{(1-f_w(s_{wO}))}{df_w/ds_w\big|_{s_{wO}}} - \frac{(1-f_w(s_{wI}))}{df_w/ds_w\big|_{s_{wI}}} \right] \tag{20}$$

From the Buckley-Leverett analysis we can remember that the gradient of the fractional flow curve at a given saturation is equal to the characteristic speed of that saturation i.e.

$$\left.\frac{df_w}{ds_w}\right|_{s_{wI}} = \left[\frac{(i-1)\Delta x}{N\Delta x}\right] \Big/ PVI \qquad \text{and} \qquad \left.\frac{df_w}{ds_w}\right|_{s_{wO}} = \left[\frac{i\Delta x}{N\Delta x}\right] \Big/ PVI \tag{21}$$

where $(i-1)\Delta x$ is the distance moved to the outlet face of the *(i-1)*th grid block $N\Delta x$ is the distance from the inlet to the outlet, *PVI* (or pore volumes injected) is the dimensionless time taken for saturation s_{wI} to reach the inlet to grid block *i* and saturation s_{wO} to reach the outlet to that grid block. Thus we can write (20) as

$$\begin{aligned}S_{wj} &= \left[s_{wI} + N \cdot PVI \frac{(1-f_w(s_{wI}))}{i-1} \right] + i(s_{wO} - s_{wI}) + N \cdot PVI \cdot i\left[\frac{(1-f_w(s_{wO}))}{i} - \frac{(1-f_w(s_{wI}))}{i-1} \right] \\ &= s_{wI} + i(s_{wO} - s_{wI}) + [(f_w(s_{wI}) - f_w(s_{wO}))]N \cdot PVI \\ &= s_{wI} + i(s_{wO} - s_{wI})\left[1 - \frac{(f_w(s_{wI}) - f_w(s_{wO}))}{(s_{wI} - s_{wO})} \frac{N}{i} PVI \right] \\ &= s_{wI} + i(s_{wO} - s_{wI})\left[1 - \frac{(f_w(s_{wI}) - f_w(s_{wO}))}{(s_{wI} - s_{wO}) df_w/ds_w\big|_{sO}} \right]\end{aligned} \tag{22}$$

where we have used equation 21

$$\frac{N \cdot PVI}{i} = \frac{1}{df_w/ds_w\big|_{sO}}$$

Equation (22) indicates that the change from point saturation value to mean saturation in the saturation tables does not depend on the number of grid blocks between producer and injector, but only the distance of the grid block from the injector (denoted by *i* in our dimensionless analysis) and the change in fractional flow across the grid block. This has been noted previously by Hewett et al (1998) however their derivation used dimensionless distance rather than fractional flow and saturation.

Examination of equations (21) also shows that if the number of grid blocks *N* is large and the grid block of interest *i* is close to the outlet at *N* then the fractional flow gradients at the inlet and outlet faces of the grid blocks will be very similar. Thus, as expected, it is most important to generate pseudos to compensate for numerical dispersion when the total number of grid blocks is small. However it also shows that it is most important to upscale relative permeability in grid blocks close to the injection well block. This was not found by the Hewett et al (1998) analysis.

In most reservoir simulations relative permeabilities are input as a table of discrete values, normally with constant intervals

Δs_w between saturations. In this case $\left.\frac{df_w}{ds_w}\right|_{sO} = \frac{f_w(s_{wj}) - f_w(s_{w(j-1)})}{s_{wj} - s_{w(j-1)}}$ where $s_{w(j-1)} < s_{wO} \le s_{wj}$. If $s_{w(j-1)} < s_{wI} \le s_{wj}$ then $s_{wj} = s_{wI}$, i.e. the saturation in the grid block is uniform and there is no need to adjust the saturations in the relative permeability curve tables (for grid blocks not containing an injection well) during pseudoisation.

Thus the only calculation needed to compensate approximately for numerical dispersion for non-well blocks is to increase the oil mobility for water saturations less than the shock front saturation. Assuming a uniform saturation behind the shock front in a given grid cell we can therefore write

$$\frac{1}{L_o} = \frac{1}{\lambda_T(s_{wf})}\frac{s_{wj} - s_{ws}}{s_{wf} - s_{ws}} + \left(1 - \frac{s_{wj} - s_{ws}}{s_{wf} - s_{ws}}\right)\frac{1}{\lambda_o(s_{wc})} \qquad (22)$$

Comparison of Pseudos with Rock Curves

Figure 3 compares the pseudo relative permeabilities generated for an injection well block and other grid blocks with the original rock curves. The corresponding total mobilities are shown in figure 4.

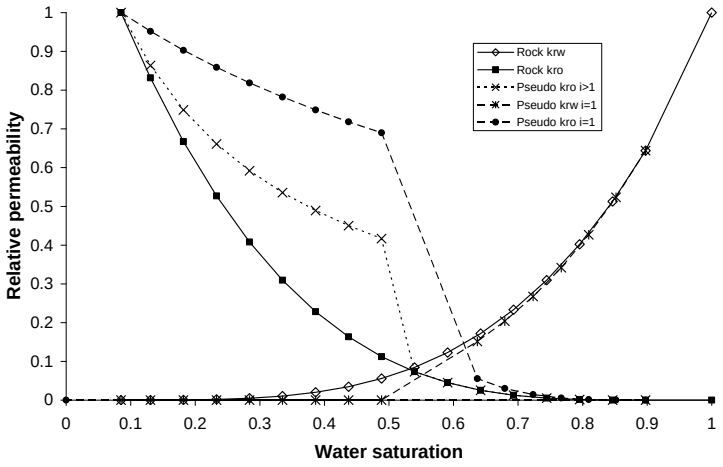

Figure 3

Comparison of pseudo curves generated for injection well block *i*=1 and other well blocks (*i*>1) with the original rock curves. The increased oil mobility for saturations below the shock front can be clearly seen as can the shift of relative permeabilities to higher water saturations for the injection well block pseudos.

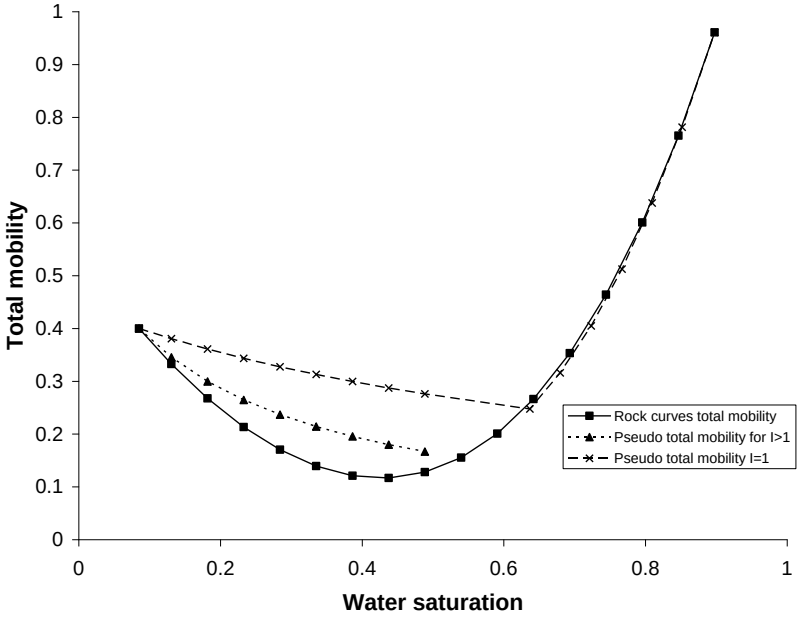

Figure 4

Comparison of pseudo total mobilities calculated using equations (13), (15) and (22) with those obtained from the rock curves shown in Figure 3

The increase in pseudo oil relative permeability for water saturation below the shock front is clear in both sets of pseudos. They remain below the oil relative permeability at S_{wc} and the rock oil relative permeability before decreasing suddenly to values close or equal to the rock curves at the shock front saturation. This is in contrast to those calculated by Hewett et al (1998) which increase to values greater than 1.

Simulation Results

Figure 5 compares the recoveries, reservoir pressures and oil rates predicted from a 1D 200 block simulation of a waterflood using the above rock curves and three coarse grid simulations, one using the rock curves and the others using the pseudo curves shown above. The coarse grid models were formed of injection and production well blocks with the same dimensions as in the fine grid simulation and five or ten blocks between these well blocks. Thus the coarse grid models had 7 or 12 grid blocks overall. The small well blocks were used to avoid issues associated with having to adjust well index to compensate for grid coarsening (see Ding and Renard. 1994; Muggeridge et al, 2002) as well as rescaling the pore volume between wells.

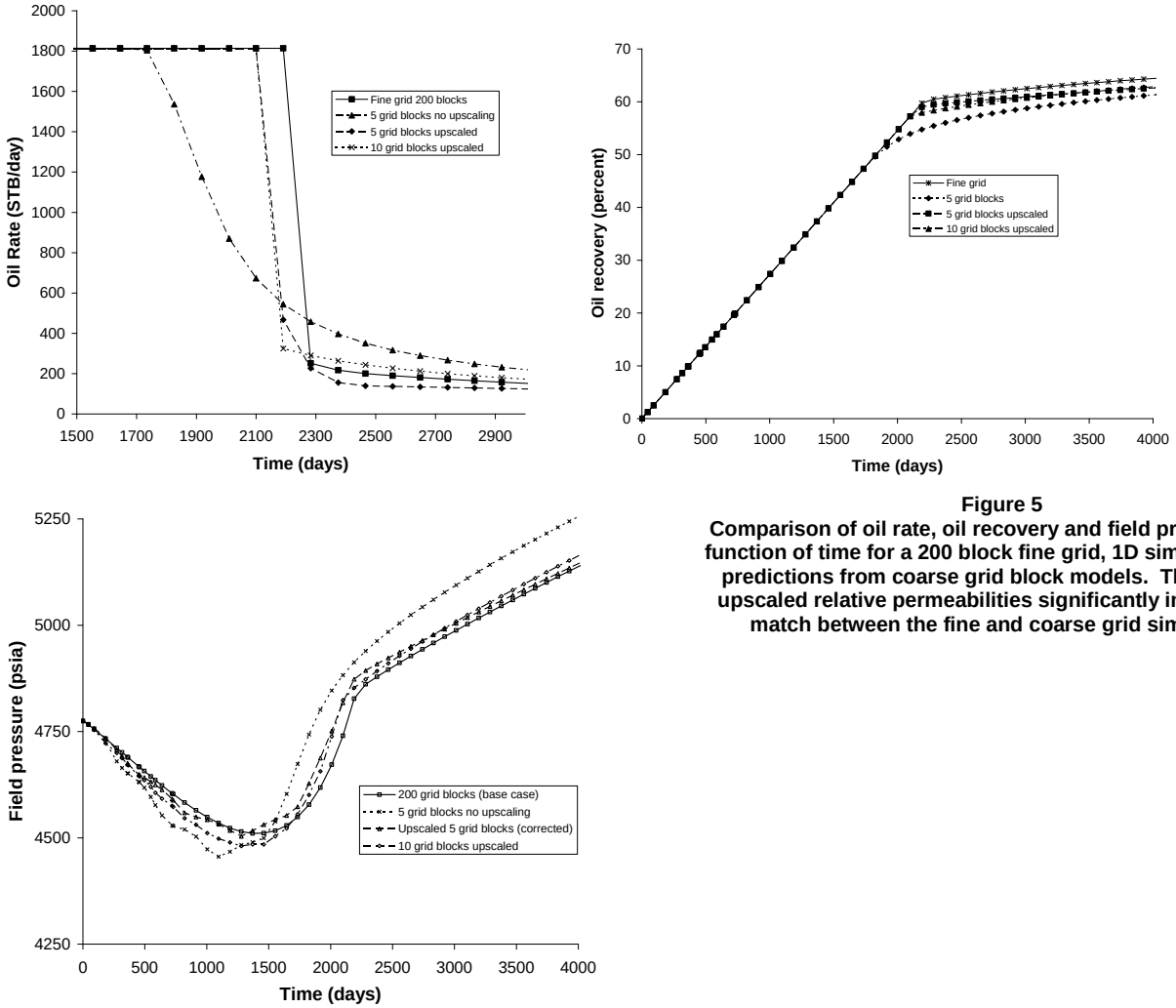

Figure 5
Comparison of oil rate, oil recovery and field pressure as a function of time for a 200 block fine grid, 1D simulation with predictions from coarse grid block models. The input of upscaled relative permeabilities significantly improve the match between the fine and coarse grid simulation

It can be seen that the upscaled models predict oil rates and field pressures much closer to those observed in the fine grid model. In particular water breakthrough is predicted only three months early in the upscaled models compared with 4 years early without upscaling. The match between fine grid simulation and upscaled models is not exact as only two pairs of pseudo relative permeabilities have been input, one for the injection well block and one for the other grid blocks. Conventional pseudoisation of this problem would result in a closer match between fine and coarse grid but would require a different set of relative permeabilities to be calculated and input for each grid block. The alternative engineering technique of simply truncating the rock curves at the shock front saturation would lead to excessively high predicted reservoir pressures in the coarse grid simulations.

Conclusions and Further Work

Buckley-Leverett analysis has been used to show that only two pairs of pseudo relative permeabilities may be needed to compensate for numerical dispersion in a homogeneous reservoir. Formulae have been presented for calculating these pseudos for a 1D line drive. The calculations suggest that more smoothly varying pseudo total mobilities will result from these formulae than were proposed by Hewett et al (1998). It would appear that Hewett et al assumed (erroneously) that total mobility was calculated by taking a harmonic mean of total mobilities at grid block boundaries rather than using upstream weighting as is normally the case.

The oil rates, recoveries and reservoir pressures predicted using the new pseudo relative permeabilities in a coarse grid 1D simulation model were compared with the fine grid results. The agreement between fine and upscaled coarse grid models is significantly better than would be obtained from using rock curves in the coarse grid model.

Further work is required to assess these pseudos in two and three-dimensional simulation. It is expected that the formulae described in this note will need to be amended for radial flow in well grid blocks. Adjustments may also be possible to model the effects of gravity on these flows.

Provided these two and three dimensional extensions work it should be possible to implement these formulae directly in the initialisation part of a reservoir simulator. The reservoir engineer could then optionally request that the simulator convert the input rock curves to pseudos that compensate for numerical dispersion, possibly including the effects of gravity (similar to the VE option in Eclipse). It should even be possible to cope with varying oil viscosity in a model by pre-calculating a range of pseudos for different water-oil mobility ratios.

References

Barker, J.W. and Dupouy, P., "An Analysis of Dynamic Relative Permeability Methods", Proceedings of the 5th European Conference on the Mathematics of Oil Recovery, Leoben, Austria, 2-6 Sept 1996.

Barker, J.W. and Thibeau, S., "A Critical Review of the Use of Pseudorelative Permeabilities for Upscaling", SPE Reservoir Engineering, p138, May 1997.

Buckley, S.E. and Leverett, M.C., "Mechanisms of Fluid Displacements in Sands", Trans. AIMME, 146, p107, 1942.

Christie, M.A., "Upscaling for Reservoir Simulation", JPT, p1004-, November 1996.

Dake, L., "Fundamentals of Reservoir Engineering", Elsevier Science 1971.

Ding, Y. and Renard, G., "A New Representation of Wells in Numerical Simulation", SPE Reservoir Engineering, pp140-144, May 1994.

Hewett, T.A., Suzuki, K. and Christie, M.A., "Analytical Calculation of Coarse-Grid Corrections for Use in Pseudofunctions", SPEJ, pp293-305, September 1998.

King, M.J., MacDonald, D.G., Todd, S.P. and Leung H., "Application of Novel Upscaling Approaches to the Magnus and Andrew Reservoirs", SPE50643, presented at the SPE European Petroleum Conference held in the Hague, The Netherlands, 20-22 October 1998.

Lantz, R.B., "Quantitative Evaluation of Numerical Diffusion", SPEJ, pp315-320, Sept 1971

Mahani, H. and Muggeridge A.H., "Improved Grid Generation Using Vorticity", SPE 94319, 14th Europec Biennial Conference held in Madrid, Spain, 13-16 June 2005.

Muggeridge A. H., " Generation of Pseudo Relative Permeabilities from Detailed Simulation of Flow in Heterogeneous Porous Media", in "Reservoir Characterisation II", Lake, L.W., Carroll, H.B. and Wesson, T.C. eds (Academic Press), 1991 (Proc. of the 2nd Int. Conf. On Reservoir Characterisation, 1989).

Muggeridge A.H., Cuypers M., Bacquet C. and Barker J.W., "Scale-up of well performance for reservoir flow simulation", Petroleum Geoscience, 8(2), pp133-139. 2002.

Welge, H.J., "A Simplified Method for Computing Oil Recovery by Gas or Water Drive", Trans. AIMME, 195, p91, 1952

Appendix D – Approximate Pseudo-relative Permeability

The following pseudorelative permeabilities for injection and non-injection well blocks are calculated by using the analytical method described in Appendix C

Table D1 – Approximate high salinity oil and water pseudo-relative permeability for injection well blocks

S_w	k_{rw}	k_{ro}	P_c
0.200	0	1.000000	0
0.220	0	0.893651	0
0.240	0	0.807748	0
0.260	0	0.736912	0
0.280	0	0.677498	0
0.300	0	0.626950	0
0.320	0	0.583421	0
0.340	0	0.545544	0
0.360	0	0.512285	0
0.380	0	0.482849	0
0.400	0	0.456611	0
0.420	0	0.433078	0
0.440	0	0.411852	0
0.460	0	0.392609	0
0.480	0	0.375085	0
0.500	0	0.359057	0
0.520	0	0.344344	0
0.540	0	0.330789	0
0.560	0	0.318260	0
0.580	0	0.306646	0
0.633	0.251405	0.024619	0
0.640	0.264463	0.020285	0
0.651	0.291570	0.013205	0
0.666	0.320000	0.008000	0
0.681	0.349752	0.004382	0
0.695	0.380826	0.002062	0
0.710	0.413223	0.000751	0
0.725	0.446942	0.000162	0
0.741	0.481983	0.000006	0
0.750	0.500000	0.000000	0

Table D2 – Approximate low salinity oil and water pseudo-relative permeability for injection well blocks

S_w	k_{rw}	k_{ro}	P_c
0.150	0	1.000000	0
0.170	0	0.890937	0
0.190	0	0.803323	0
0.210	0	0.731399	0
0.230	0	0.671295	0
0.250	0	0.620320	0
0.270	0	0.576540	0
0.290	0	0.538532	0
0.310	0	0.505225	0
0.330	0	0.475799	0
0.350	0	0.449611	0
0.370	0	0.426156	0
0.390	0	0.405027	0
0.410	0	0.385894	0
0.430	0	0.368487	0
0.450	0	0.352583	0
0.470	0	0.337994	0
0.490	0	0.324565	0
0.510	0	0.312163	0
0.530	0	0.300673	0
0.550	0	0.289999	0
0.570	0	0.280057	0
0.590	0	0.270774	0
0.610	0	0.262087	0
0.630	0	0.253940	0
0.650	0	0.246284	0
0.670	0	0.239076	0
0.690	0	0.232278	0
0.700	0	0.229022	0
0.763	0.195129	0.016258	0
0.774	0.209316	0.011646	0
0.788	0.224000	0.008000	0
0.802	0.239182	0.005208	0
0.817	0.254862	0.003155	0
0.832	0.271040	0.001728	0
0.846	0.287716	0.000813	0
0.861	0.304889	0.000296	0
0.875	0.322560	0.000064	0
0.891	0.340729	0.000002	0
0.900	0.350000	0.000000	0

Table D3 – Approximate high salinity oil and water pseudo-relative permeability for non-injection well blocks

S_w	k_{rw}	k_{ro}	P_c
0.20	0	1.000000	0
0.22	0	0.866047	0
0.24	0	0.763741	0
0.26	0	0.683053	0
0.28	0	0.617785	0
0.30	0	0.563902	0
0.32	0	0.518664	0
0.34	0	0.480145	0
0.36	0	0.446952	0
0.38	0	0.418052	0
0.40	0	0.392662	0
0.42	0	0.370180	0
0.44	0	0.350132	0
0.46	0	0.332145	0
0.48	0	0.315915	0
0.50	0	0.301198	0
0.52	0	0.287791	0
0.54	0	0.275526	0
0.56	0	0.264264	0
0.58	0	0.253887	0
0.59	0.251405	0.024619	0
0.60	0.264463	0.020285	0
0.62	0.291570	0.013205	0
0.64	0.320000	0.008000	0
0.66	0.349752	0.004382	0
0.68	0.380826	0.002062	0
0.70	0.413223	0.000751	0
0.72	0.446942	0.000162	0
0.74	0.481983	0.000006	0
0.75	0.500000	0.000000	0

Table D4 – Approximate low salinity oil and water pseudo-relative permeability for non-injection well blocks

S_w	k_{rw}	k_{ro}	P_c
0.15	0	1.000000	0
0.17	0	0.870119	0
0.19	0	0.770099	0
0.21	0	0.690702	0
0.23	0	0.626147	0
0.25	0	0.572627	0
0.27	0	0.527536	0
0.29	0	0.489028	0
0.31	0	0.455759	0
0.33	0	0.426729	0
0.35	0	0.401175	0
0.37	0	0.378509	0
0.39	0	0.358267	0
0.41	0	0.340081	0
0.43	0	0.323651	0
0.45	0	0.308736	0
0.47	0	0.295135	0
0.49	0	0.282682	0
0.51	0	0.271237	0
0.53	0	0.260683	0
0.55	0	0.250919	0
0.57	0	0.241860	0
0.59	0	0.233433	0
0.61	0	0.225573	0
0.63	0	0.218225	0
0.65	0	0.211341	0
0.67	0	0.204878	0
0.69	0	0.198798	0
0.70	0	0.195892	0
0.71	0.195129	0.016258	0
0.73	0.209316	0.011646	0
0.75	0.224000	0.008000	0
0.77	0.239182	0.005208	0
0.79	0.254862	0.003155	0
0.81	0.271040	0.001728	0
0.83	0.287716	0.000813	0
0.85	0.304889	0.000296	0
0.87	0.322560	0.000064	0
0.89	0.340729	0.000002	0
0.90	0.350000	0.000000	0

Appendix E – Upscaling for the Simulation of Low Salinity Waterflooding: Salinity Thresholds by Ann H. Muggeridge (November 2007)

Introduction

Low salinity water injection is only effective when the salinity of the water in contact with the oil is below a threshold value (Jerauld, 2005; Jerauld et al 2006). Below this threshold oil recovery will increase as the water salinity decreases until at a lower salinity threshold no further improvement in oil recovery is observed. Thus low salinity water flooding is modelled in numerical simulation using an upper and lower salinity threshold to control whether high or low salinity relative permeability curves are used in a given grid block.

During a water flood the injected and connate water mix through molecular diffusion and advective dispersion. This mixing occurs on the pore scale due to the tortuosity of the pore network (Perkins and Johnston, 1963) and on larger scales to heterogeneity in permeability in the reservoir (Arya et al, 1988; Mahadevan et al, 2005). Thus if the connate water is of a different (usually higher if a low salinity waterflood is being modelled) salinity than the injected water the salinity of the water in contact with the oil will vary as a function of distance and time from injection according to the diffusion equation:

$$\frac{\partial c}{\partial t} = -\mathbf{K}\nabla^2 c \qquad (1)$$

where c is the concentration of salt in the water, t is time (seconds) and $\mathbf{K}$ is the dispersion tensor ($m^2\ s^{-1}$). As a result the front between injected low salinity water and connate higher salinity water will be dispersed, thus there will be a later breakthrough of the additional oil from the low salinity displacement and possibly a lower recovery if only a slug of low salinity water is injected.

During conventional finite difference simulation, artificial mixing may also occur due to time and space truncation errors resulting from approximating the partial differential equations by linear gradients. This is termed numerical dispersion and has been analysed by a number of authors including Lantz (1971). The level of numerical dispersion in a given simulation will increase as the number of grid blocks decreases. It is possible to replicate the effects of physical diffusion and dispersion by choosing grid dimensions so that the resulting numerical dispersion is of the same magnitude as the physical dispersion (see Jerauld, 2005). This can be advantageous when using a reservoir simulator that does not model physical diffusion and dispersion. However in many cases engineers are forced to use coarser grids in order to able to run field scale simulations within realistic time-scales.

As a result the levels of numerical dispersion may far exceed the expected levels of physical dispersion. In the case of low salinity water injection this will cause artificially high mixing between low salinity injected and high salinity connate water, resulting in the simulator calculating high salinity water (above the thresholds) in contact with the oil and pessimistic predictions of oil recovery.

This note describes a simple method for calculating pseudo low and high salinity thresholds that compensate for excess numerical dispersion in coarse grid simulations, allowing more realistic predictions of oil recovery in these cases.

Theory

Consider the situation where low salinity water (concentration c_L) is displacing high salinity water (concentration c_R). If we neglect the oil saturation and thus the complexities of two-phase, Darcy Flow, and assume the initial conditions are

$$c(x,0) = C_L \qquad -\infty < x < 0$$
$$c(x,0) = C_R \qquad 0 < x < \infty$$

then the solution to equation (1) for the concentration of salinity across the interface between the two waters is (ref):

$$c(x,t) = \langle C \rangle + \frac{\Delta C}{2}\,\mathrm{erf}\left(\frac{x}{\sqrt{4Dt}}\right) \qquad (2)$$

where

$$\langle C \rangle = \frac{C_L + C_R}{2}$$
$$\Delta C = C_R - C_L$$

x is distance (m), t is time (s) and D is the diffusion (dispersion) coefficient ($m^2\ s^{-1}$). This is illustrated in figure 1.

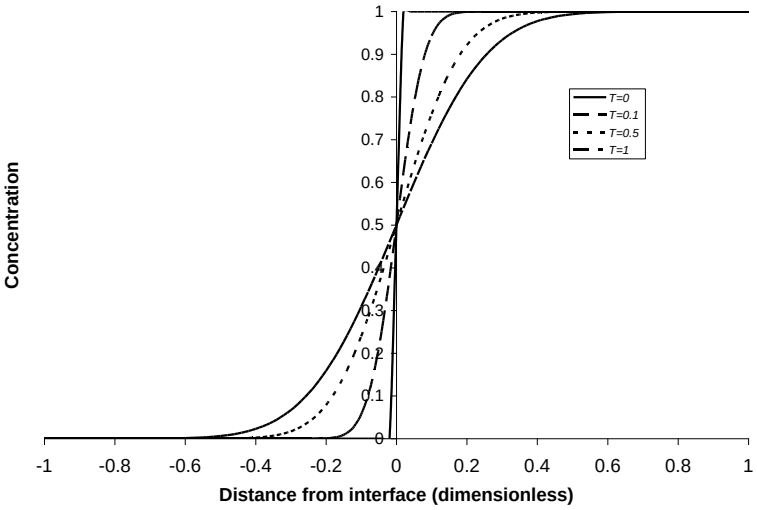

Figure 1
An initially sharp front will spread over time due to diffusion and dispersion.

Note that we have assumed that the mixing across the interface is independent of the movement of the water front through the reservoir. This is effectively assuming that the water viscosity is not dependent on salinity. It also assumes that mixing is not influenced by the reservoir boundaries. Alternative analytical solutions could be used for these cases, but as we shall show these effects are small and can be neglected.

In order to non-dimensionalize the above equation we write $X = \frac{x}{L} \text{ and } \tau = \frac{t}{T}$

where L is the interwell spacing (m) and T is the time taken for the front to travel from injection to production well i.e. $T = \frac{L}{v}$ (s) where v is velocity of the front (m s^{-1}). Thus we can re-write equation (2) as

$$c(x,t) = \langle C \rangle + \frac{\Delta C}{2} \text{erf}\left(\sqrt{\frac{Lv}{4D}} \frac{X}{\sqrt{t}} \right) \tag{3}$$

On the field scale mixing is dominated by advective dispersion so we can write $D \approx \alpha v$ where α is the dispersion coefficient (m). If the displacement is dominated by numerical dispersion then we can write $\frac{\alpha}{L} = \frac{1}{2N}$ (Jerauld, 2005) where N is the number of grid blocks between wells. Substituting in the above equation we get

$$c(x,t) = \langle C \rangle + \frac{\Delta C}{2} \text{erf}\left(\sqrt{\frac{N}{2}} \frac{X}{\sqrt{t}} \right) \tag{4}$$

As discussed above the effect of using a coarser grid is to increase levels of numerical dispersion. This will result in water salinity rising above the threshold values for low salinity to be effective sooner than would actually be the case. Figure 2 shows the salinity distribution at a given time for a 25 grid block and 5 grid block simulation model together with the physical values for lower and upper salinity thresholds (2000ppm and 8000ppm in this case). In order to replicate the special locations in the reservoir where low salinity becomes effective we need to alter the lower and upper salinity thresholds as shown by the construction in figure 2. In the case illustrated the pseudo upper salinity threshold is ~40,000ppm and the pseudo lower salinity threshold is ~25,000ppm.

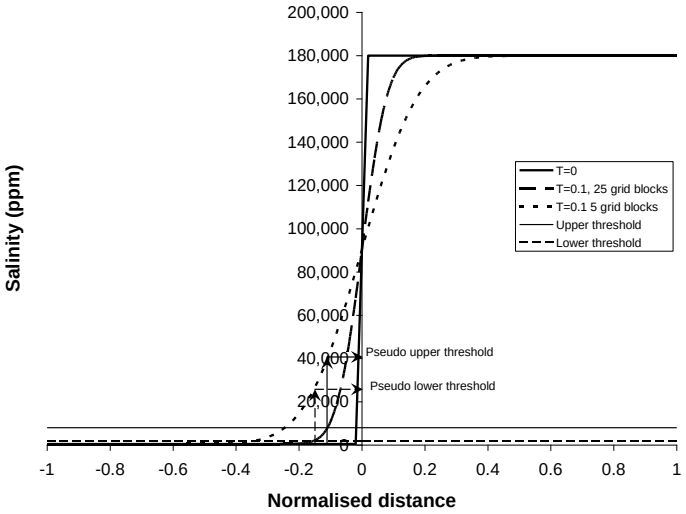

Figure 2
The dashed line shows the spreading of a front between low and high salinity water expected from a simulation model with 25 grid blocks between wells. The line with shorter dashes shows the increased spreading that would be observed if there were only 5 grid blocks between wells. The arrows show the change in lower and upper salinity thresholds required to predict the transition from low salinity to high salinity relative permeabilities at the same time and space in the simulation.

These values can also be calculated as follows. First we normalise salinity threshold c_T between the injected and connate values to give:

$$C_T = \frac{2\left(c_T - \langle C \rangle\right)}{\Delta C} = \mathrm{erf}\left(\frac{X}{\sqrt{\tau}}\sqrt{\frac{N}{2}}\right) \tag{5}$$

The data in figure 2 was generated assuming a connate water salinity of 180,000ppm and an injected water salinity of 500ppm. Taking the lower salinity threshold (2000ppm), this means that C_T=0.983 so, using a standard error function table,

$$\frac{X}{\sqrt{\tau}} = 1.69\sqrt{\frac{2}{N}} \tag{6}$$

For upscaling we need to calculate a pseudo threshold salinity that will move through the reservoir in the same way as the physical salinity threshold ie we need to preserve $\frac{X}{\sqrt{\tau}}$. Thus we can write the normalised pseudo salinity threshold C_{PT} for a coarse grid size N_C as

$$C_{PT} = \frac{2\left(\langle C \rangle - c_{PT}\right)}{\Delta C} = \mathrm{erf}\left(1.69\sqrt{\frac{N_C}{N}}\right) \tag{7}$$

If there are 5 grid blocks between wells in the coarse grid simulation and the physical dispersion is equivalent to a grid with 25 blocks between wells this results in a pseudo lower salinity threshold of 26,100ppm. Following the same procedure for the upper salinity threshold we get a pseudo upper threshold of 40,000 ppm. Table 1 shows how pseudo lower and upper salinity thresholds change with connate salinity assuming an injected water salinity of 500ppm and a physical lower threshold of 2000ppm and an upper threshold of 8000ppm.

Connate salinity (ppm)	Physical salinity threshold (ppm)	Pseudo salinity threshold (ppm)
33,000	2,000	7.840
	8,000	12,560
180,000	2,000	26,100
	8,000	40,000
250,000	2,000	33,000
	8,000	50,400

Table 1
This shows the effect of connate salinity on pseudo salinity threshold when moving from 25 grid blocks between wells to 5 grid blocks between wells. It can be seen that the higher the connate salinity the higher the pseudo salinity thresholds.

Example Results

The above procedure was tested on two secondary low salinity water floods: one continuous and the other modelling the injection of a 0.33 PV slug of low salinity brine. In both cases the connate brine salinity was 33,000ppm and the injected low salinity brine salinity was 500ppm. The physical lower and upper salinity thresholds were 2000ppm and 8000ppm respectively. In each flood it was assumed that the physical dispersion was correctly represented by simulating the displacement with 25 grid blocks between wells.

Table 2 summarises the different 1D simulations performed. The coarse grid runs used a grid formed of 5 coarse grid blocks between the injector and producer well blocks. The injector and producer well blocks were retained with the same dimensions as in the fine, 25 grid block runs in order to remove the need for upscaling of well index (Ding, 1994; Muggeridge et al, 2002). Thus the total number of grid blocks in the coarse grid simulations was 7.

Low salinity injection scheme	No. of grid blocks	Lower threshold (ppm)	Upper threshold (ppm)	Inaccessible water?
Continuous	25	2000	8000	No
	25	2000	8000	Yes
	7	2000	8000	No
	7	2000	8000	Yes
	7	7840	12560	No
0.33PV Slug	25	2000	8000	No
	7	2000	8000	No
	7	7840	12560	No

Table 2

Summary of input parameters for various 1D, line drive simulations performed to test the proposed algorithm for upscaling salinity thresholds. Note that the 7 grid block runs consisted of an injection well block and a production well block of the same dimensions as those blocks in the fine grid, 25 cell simulations plus 5 coarse grid blocks. The amount of inaccessible water in the runs where that option was turned on was equal to the connate water saturation.

Figure 3 compares the recoveries predicted by the different simulations of continuous low salinity water injection and Figure 4 shows the produced oil rates versus time. As expected the fine grid run with inaccessible connate water gives the maximum recovery as there is no mixing between the injected water and the connate water. Thus all the mobile water is below the low salinity threshold. In this case the low salinity relative permeablities are used throughout the displacement. The next highest recovery is obtained with the fine grid simulation with all the connate water accessible for mixing with the injected water. In this case there is a transition from high salinity relative permeability curves to low salinity relative permeabilities resulting in the development of an oil 'bank' which is produced after water breakthrough (see figure 4). It is assumed that this simulation correctly reproduces the effect of field scale mixing on low salinity oil recovery.

Figure 3 also shows that the coarse grid simulation using the physical salinity thresholds and making all the connate water available for mixing gives the lowest oil recovery and the earliest water breakthrough. The two coarse runs a) using physical threshold values and inaccessible water and b) upscaled thresholds with connate water available for mixing give more or less identical recovery curves and oil rates versus time. They both predict approximately the correct time for water breakthrough and initial oil recovery versus time after breakthrough. However the later cumulative oil recovery is underpredicted, although better than that predicted by the coarse grid run allowing complete mixing between connate water and injected water.

Examination of figure 4 shows that although the coarse grid simulation with accessible water and physical salinity thresholds underpredicts oil recovery it does at least approximate the development of the low salinity oil bank seen in the fine grid simulation.

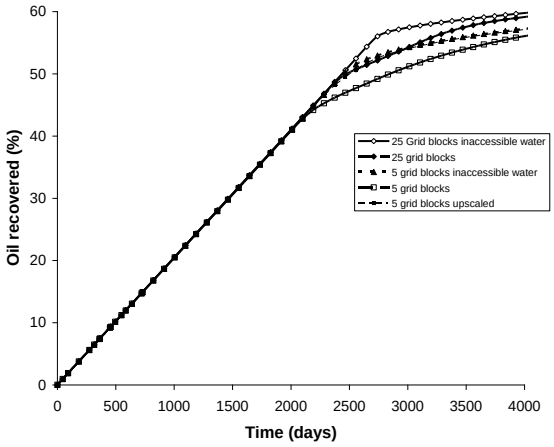

Figure 3

Comparison of cumulative oil recovery as a function of time for continuous low salinity water injection. The parameters used in the fine and coarse grid simulations are summarised in Table 2. It can be seen that both the coarse grid model using upscaled salinity thresholds and the coarse grid model using inaccessible water give a fair approximation to the oil recovery obtained from the fine grid simulation with accessible water.

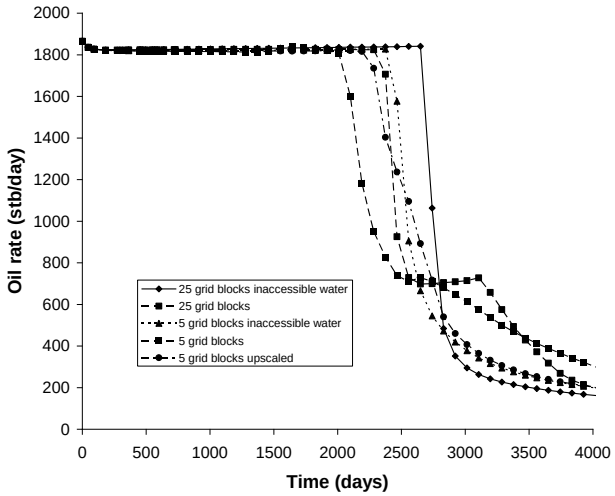

Figure 4
Comparison of oil rate as a function of time for continuous low salinity water injection. The parameters used in the fine and coarse grid simulations are summarised in Table 2. It can be seen that both the coarse grid model using upscaled salinity thresholds and the coarse grid model using inaccessible water give a fair approximation to the oil rate obtained from the fine grid simulation with accessible water. However they do not predict the oil bank seen in the fine grid simulation with accessible connate water and the coarse grid simulation using physical salinity thresholds and accessible connate water.

These results suggest that there needs to relative permeability upscaling to compensate for numerical dispersion as well as upscaling of salinity thresholds.

Figures 5 and 6 show the cumulative oil recovery and oil rates versus time for the simulations of injection of a 0.33PV low salinity slug. In all cases the connate water was accessible for mixing with the injected water. Again it can be seen that the coarse grid simulation using upscaled salinity thresholds gives a much better estimate of fine grid oil recovery versus time compared to the coarse grid simulation using physical salinity thresholds. It also gives a better estimate of water breakthrough and initial oil rate decline although again it fails to predict the arrival of the oil bank at around 3000days. Again this suggests that additional upscaling of the relative permeabilities is needed to predict the complete low salinity recovery process.

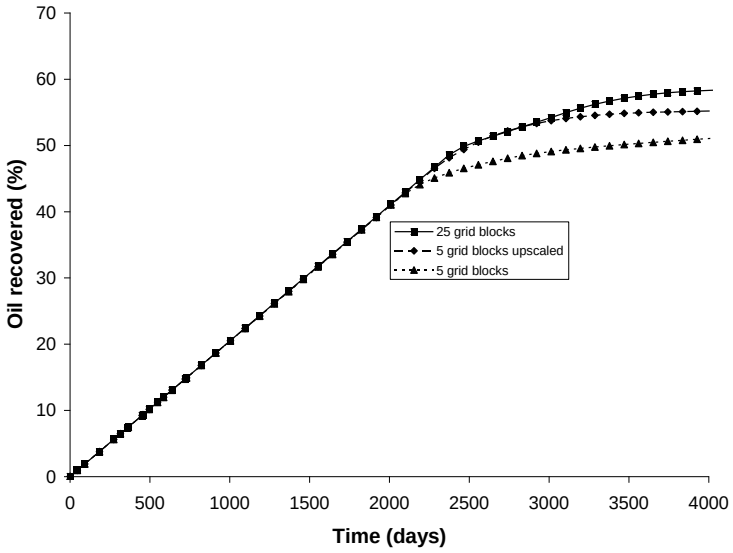

Figure 5
Comparison of cumulative oil recovery as a function of time when a 0.33 PV slug of low salinity water is injected. The parameters for fine and coarse grid simulations are summarised in Table 2. It can be seen that the coarse grid model using upscaled salinity thresholds gives a fair approximation to the oil recovery obtained from the fine grid simulation.

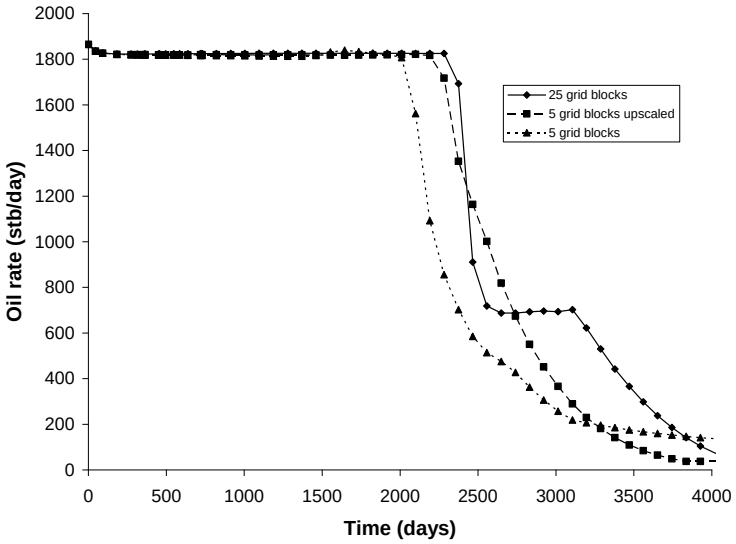

Figure 6
Comparison of oil rate as a function of time when a 0.33 PV slug of low salinity water is injected. The parameters used in the fine and coarse grid simulations are summarised in Table 2. It can be seen that the coarse grid model using upscaled salinity thresholds gives a fair approximation to the oil rate up to 2750 days obtained from the fine grid simulation. However it does not predict the oil bank seen in the fine grid simulation.

Conclusions

This note describes a simple way of upscaling lower and upper salinity thresholds to compensate for excessive numerical dispersion in coarse grid simulation models. The efficacy of this method has been demonstrated for secondary low salinity water injection for both continuous and slug injection when upscaling from 25 grid blocks to 5 grid blocks between injector and producer.

Particular observations are that

- The difference between the physical and upscaled salinity thresholds increases as the salinity of the connate water increases.
- The simulations using upscaled salinity thresholds correctly predict early oil rate and water breakthrough but do not predict the later arrival of an oil bank
- The use of inaccessible water can also be used to upscale the displacements investigated here. However it is unlikely to work for tertiary low salinity floods.

Further work is needed to upscale the relative permeabilities to predict the later arrival of an oil bank. This will be the subject of another note.

References

Arya, A., Hewett, T.A., Larson, R.G. and Lake L.W., "Dispersion and Reservoir Heterogeneity", SPE Reservoir Engineering, February 1988

Ding, Y. and Renard, G., "A New Representation of Wells in Numerical Simulation", SPE Reservoir Engineering, pp140-144, May 1994.

Jerauld, G.R, "Low salinity Simulation Users Manual", BP Internal Report, December 2005

Jerauld, G.R., Lin, C.Y., Webb, K.J. and Seccombe J.C., "Modelling Low-Salinity Waterflooding", SPE 102239, presented at the 2006 SPE Annual Technical Conference and Exhibition held in San Antonio Texas.

Lantz, R.B., "Quantitative Evaluation of Numerical Diffusion", SPEJ, pp315-320, Sept 1971.

Mahadevan, J. Lake, L.W. and Johns, R.T., "Estimation of the True Dispersivity in Field-Scale Permeable Media, SPE86303, 2003.

Muggeridge A.H., Cuypers M., Bacquet C. and Barker J.W., "Scale-up of well performance for reservoir flow simulation", Petroleum Geoscience, 8(2), pp133-139. 2002.

Perkins, T.K. and Johnston, O.C., "A Review of Diffusion and Dispersion in Porous Media", SPEJ, pp70-84, March 1963

Appendix F – Example Eclipse Data Files for Low Salinity Waterflood Simulation

F.1 Eclipse data file for 1D fine-grid low salinity waterflood simulation

```
RUNSPEC
=========================================================================================================
TITLE
 LoSal Water injection Fine grid /

DIMENS
   98   1    1  /
OIL
WATER
GAS
LOWSALT
METRIC
TABDIMS
    2    1   50   20    1   20 /
WELLDIMS
    3    10    1    3 /
START
   1 'JAN' 1990  /
UNIFIN
UNIFOUT
ACTDIMS
10 /
UDQDIMS
--MAX NO.     MAX NO.   MAX NO.     MAX NO.  MAX   MAX   MAX     MAX   MAX      MAX
--FUNCTIONS   ARGUMNTS  CONECTION   FIELD    GRUP  REGN  SEGMNT  WELL  AQUIFER  BLOCK
    12           12        2          10        0     4    0      10    0        4  /
UDQPARAM
-- SEED  RANGE  UNDEFINEDVALUE  TOLERANCE
    1     1e19     -2.5         1.0E-4     /
UDADIMS
20  /
--NOSIM

GRID      ================================================================

INIT
DX
  10.41667 96*10.41667 10.41667  /
DY
  98*100   /
DZ
  98*50   /
PERMX
  98*100   /
COPY
 PERMX  PERMY  /
 PERMX  PERMZ  /
/
MULTIPLY
PERMZ 0.1 /
/
PORO
  98*0.20   /
TOPS
 98*2600 /

PROPS     ================================================================
LSALTFNC
0.0     1  1*
1.0     1  1*
7.0     0  1*
30.0    0  1*
/
/
SWOF
-- SL = SWCR = 0.2   High salinity curves
--   Sw   Krw   Pwo
0.2    0.0000000      1.0000000      0
0.22   0.0006612      0.8948279      0
0.24   0.0026446      0.7973013      0
0.26   0.0059504      0.7071315      0
```

```
0.28    0.0105785       0.6240301       0
0.3     0.0165289       0.5477085       0
0.32    0.0238017       0.4778783       0
0.34    0.0323967       0.4142509       0
0.36    0.0423140       0.3565379       0
0.38    0.0535537       0.3044508       0
0.4     0.0661157       0.2577010       0
0.42    0.0800000       0.2160000       0
0.44    0.0952066       0.1790594       0
0.46    0.1117355       0.1465905       0
0.48    0.1295868       0.1183050       0
0.5     0.1487603       0.0939144       0
0.52    0.1692562       0.0731300       0
0.54    0.1910744       0.0556634       0
0.56    0.2142149       0.0412261       0
0.58    0.2386777       0.0295297       0
0.6     0.2644628       0.0202855       0
0.62    0.2915702       0.0132051       0
0.64    0.3200000       0.0080000       0
0.66    0.3497521       0.0043817       0
0.68    0.3808264       0.0020616       0
0.7     0.4132231       0.0007513       0
0.72    0.4469421       0.0001623       0
0.74    0.4819835       0.0000060       0
0.75    0.5000000       0.0000000       0
/
-- low salinity   or
-- Sw   Krw                     Kro
0.15    0.0000000       1.0000000       0
0.17    0.0002489       0.9221144       0
0.19    0.0009956       0.8483816       0
0.21    0.0022400       0.7786880       0
0.23    0.0039822       0.7129197       0
0.25    0.0062222       0.6509630       0
0.27    0.0089600       0.5927040       0
0.29    0.0121956       0.5380290       0
0.31    0.0159289       0.4868243       0
0.33    0.0201600       0.4389760       0
0.35    0.0248889       0.3943704       0
0.37    0.0301156       0.3528936       0
0.39    0.0358400       0.3144320       0
0.41    0.0420622       0.2788717       0
0.43    0.0487822       0.2460990       0
0.45    0.0560000       0.2160000       0
0.47    0.0637156       0.1884610       0
0.49    0.0719289       0.1633683       0
0.51    0.0806400       0.1406080       0
0.53    0.0898489       0.1200664       0
0.55    0.0995556       0.1016296       0
0.57    0.1097600       0.0851840       0
0.59    0.1204622       0.0706157       0
0.61    0.1316622       0.0578110       0
0.63    0.1433600       0.0466560       0
0.65    0.1555556       0.0370370       0
0.67    0.1682489       0.0288403       0
0.69    0.1814400       0.0219520       0
0.71    0.1951289       0.0162584       0
0.73    0.2093156       0.0116456       0
0.75    0.2240000       0.0080000       0
0.77    0.2391822       0.0052077       0
0.79    0.2548622       0.0031550       0
0.81    0.2710400       0.0017280       0
0.83    0.2877156       0.0008130       0
0.85    0.3048889       0.0002963       0
0.87    0.3225600       0.0000640       0
0.89    0.3407289       0.0000024       0
0.90    0.3500000       0.0000000       0
/
SGOF
-- High salinity curves
-- SG           Krg                     Kro                     Pc
0.00    0.000           1.000           0.000
0.08    0.001           0.729           0.000
0.16    0.005           0.512           0.000
0.24    0.016           0.343           0.000
0.32    0.038           0.216           0.000
```

```
0.40    0.075          0.125          0.000
0.48    0.130          0.064          0.000
0.56    0.206          0.027          0.000
0.64    0.307          0.008          0.000
0.72    0.437          0.001          0.000
0.80    0.600          0.000          0.000
/
-- Low salinity curves
0.00    0.000          1.000          0.000
0.09    0.005          0.810          0.000
0.17    0.020          0.640          0.000
0.26    0.045          0.490          0.000
0.34    0.080          0.360          0.000
0.43    0.125          0.250          0.000
0.51    0.180          0.160          0.000
0.60    0.245          0.090          0.000
0.68    0.320          0.040          0.000
0.77    0.405          0.010          0.000
0.85    0.500          0.000          0.000
/
PVDO
  200    1.0     0.47
  280    0.999   0.47
  300    0.998   0.47
/
PVDG
--   PGAS   BGAS              VISGAS
10.00000               0.12668        0.01316
35.78947               0.03436        0.01361
61.57895               0.01944        0.01426
87.36842               0.01340        0.01506
113.15789              0.01017        0.01601
138.94737              0.00820        0.01711
164.73684              0.00689        0.01832
190.52632              0.00599        0.01962
216.31579              0.00533        0.02097
242.10526              0.00484        0.02234
270.00000              0.00444        0.02383
293.68421              0.00417        0.02507
319.47368              0.00393        0.02640
345.26316              0.00374        0.02770
371.05263              0.00358        0.02896
396.84211              0.00344        0.03019
422.63158              0.00332        0.03138
448.42105              0.00322        0.03254
474.21053              0.00313        0.03367
500.00000              0.00305        0.03476
/
ROCK
 270 .3E-5 /
DENSITY
-- o   w    g
 850. 1000. 1.2 /
PVTWSALT
 270.0 0.0/
 0.0  1.030  4.6E-5  0.5  0.0
10.0  1.030  4.6E-5  0.5  0.0 /

REGIONS    ============================================================

SATNUM
-- immiscible, high salinity = 1
 98*1 /
LWSLTNUM
-- low salinity curves
 98*2
/
RPTREGS
 24*0 /
RPTREGS
SURFNUM LWSLTNUM LSLTWNUM /

SOLUTION   ============================================================

EQUIL
-- Datum   Pressure   WOC
```

```
2680       270        2680 1*  2000/
SALTVD
 5000.0  30.0
 5500.0  30.0 /
RPTRST
'BASIC=2'  /

SUMMARY    ============================================================
FSPR
FSPT
FSIR
FSIT
FWIR
FOPR
FGPR
FOPT
FPR
FOPV
FWIT
FOE
TCPU
GSPR
 'G' /
GSPT
 'G' /
GSIR
 'G' /
GSIT
 'G' /
GSPR
 'G' /
WSPR
 'OP' /
WSPT
 'OP' /
WSIR
'INJ' /
WSIT
'OP ' /
WBHP /
WOPR
'OP' /
WGPR
'OP' /
WLPR
'OP' /
WWPR
'OP' /
WWCT
'OP' /
WWIR
'INJ'/
CSFR
 'OP'  98 1 1 /      con. salt flow rate (+/-)
 'INJ'  1 1 1 /
/
CSPT
 'OP'  98 1 1 /
/
CSIT
 'INJ'  1 1 1 /
/
BSCN
 1 1 1 /
 2 1 1 /
 4 1 1 /
 6 1 1 /
 8 1 1 /
10 1 1 /
12 1 1 /
14 1 1 /
16 1 1 /
18 1 1 /
20 1 1 /
22 1 1 /
24 1 1 /
```

```
26 1 1 /
28 1 1 /
30 1 1 /
32 1 1 /
34 1 1 /
36 1 1 /
38 1 1 /
40 1 1 /
42 1 1 /
44 1 1 /
46 1 1 /
48 1 1 /
50 1 1 /
52 1 1 /
54 1 1 /
56 1 1 /
58 1 1 /
60 1 1 /
62 1 1 /
64 1 1 /
66 1 1 /
68 1 1 /
70 1 1 /
72 1 1 /
74 1 1 /
76 1 1 /
78 1 1 /
80 1 1 /
82 1 1 /
84 1 1 /
86 1 1 /
88 1 1 /
90 1 1 /
92 1 1 /
94 1 1 /
96 1 1 /
98 1 1 /
/
BSIP
 1 1 1 /
 2 1 1 /
20 1 1 /
40 1 1 /
60 1 1 /
80 1 1 /
97 1 1 /
98 1 1 /
/
BPR
 1 1 1 /
 2 1 1 /
20 1 1 /
40 1 1 /
60 1 1 /
80 1 1 /
97 1 1 /
98 1 1 /
/
BOSAT
 1 1 1 /
 2 1 1 /
20 1 1 /
40 1 1 /
60 1 1 /
80 1 1 /
97 1 1 /
98 1 1 /
/
BGSAT
 1 1 1 /
 2 1 1 /
20 1 1 /
40 1 1 /
60 1 1 /
80 1 1 /
97 1 1 /
```

```
98 1 1 /
/
BWSAT
 1 1 1 /
 2 1 1 /
 4 1 1 /
 6 1 1 /
 8 1 1 /
10 1 1 /
12 1 1 /
14 1 1 /
16 1 1 /
18 1 1 /
20 1 1 /
22 1 1 /
24 1 1 /
26 1 1 /
28 1 1 /
30 1 1 /
32 1 1 /
34 1 1 /
36 1 1 /
38 1 1 /
40 1 1 /
42 1 1 /
44 1 1 /
46 1 1 /
48 1 1 /
50 1 1 /
52 1 1 /
54 1 1 /
56 1 1 /
58 1 1 /
60 1 1 /
62 1 1 /
64 1 1 /
66 1 1 /
68 1 1 /
70 1 1 /
72 1 1 /
74 1 1 /
76 1 1 /
78 1 1 /
80 1 1 /
82 1 1 /
84 1 1 /
86 1 1 /
88 1 1 /
90 1 1 /
92 1 1 /
94 1 1 /
96 1 1 /
98 1 1 /
/
BWVIS
 1 1 1 /
 2 1 1 /
20 1 1 /
40 1 1 /
60 1 1 /
80 1 1 /
97 1 1 /
98 1 1 /
/
BOKR
 1 1 1 /
 2 1 1 /
20 1 1 /
40 1 1 /
60 1 1 /
80 1 1 /
97 1 1 /
98 1 1 /
/
BGKR
 1 1 1 /
```

```
 2 1 1 /
20 1 1 /
40 1 1 /
60 1 1 /
80 1 1 /
97 1 1 /
98 1 1 /
/
BWKR
 1 1 1 /
 2 1 1 /
20 1 1 /
40 1 1 /
60 1 1 /
80 1 1 /
97 1 1 /
98 1 1 /
/
BWKR
 1 1 1 /
 2 1 1 /
20 1 1 /
40 1 1 /
60 1 1 /
80 1 1 /
97 1 1 /
98 1 1 /
/
FUHCPVI
RPTONLY
ALL
SEPARATE
RUNSUM
MSUMLINS
MSUMNEWT

SCHEDULE   ============================================================

TUNING
1 30 /
 /
 /
WELSPECS
'OP'   'G'   98 1  2600  'OIL'  /
'INJ'  'G'   1  1  2600  'WAT'  /
/
COMPDAT
'OP      '   98   1   1   1  'OPEN'   0  .0   157E-3 /
'INJ     '   1    1   1   1  'OPEN'   0  .0   157E-3 /
/
WCONPROD
'OP' 'OPEN' 'RESV' 4* 304.8 0.0 7* /
/
WCONINJE
'INJ'  'WAT' 'OPEN' 'RESV' 1* 304.8 /
/
UDQ
DEFINE FUHCPV FOPV /
UPDATE FUHCPV NEXT /
/
WCONPROD
'OP' 'OPEN' 'RESV' 4* 304.8 0.0 7* /
/
WCONINJE
'INJ'  'WAT' 'OPEN' 'RESV' 1* 304.8 /
/
UDQ
DEFINE FUHCPVI FWIT/FUHCPV /
/
WSALT
INJ 1 /
/
TSTEP
228*30 /

END
```

F.2 Eclipse data file for 1D coarse-grid low salinity waterflood simulation with upscaled properties

```
RUNSPEC
=========================================================================================================
TITLE
 Upscaled LoSal Water injection 3GB, PVW kr, threshold 3,700-10,800 /

DIMENS
   5   1    1  /

OIL
WATER
LOWSALT
METRIC

TABDIMS
    8    1   100   20    1   20 /
WELLDIMS
    3    10    1    3 /
START
   1 'JAN' 1990  /
UNIFIN
UNIFOUT
ACTDIMS
10 /
UDQDIMS
--MAX NO.      MAX NO.   MAX NO.      MAX NO.  MAX   MAX   MAX      MAX   MAX       MAX
--FUNCTIONS   ARGUMNTS  CONECTION    FIELD    GRUP  REGN  SEGMNT  WELL  AQUIFER  BLOCK
    12           12         2           10        0     4     0      10    0         4  /
UDQPARAM
-- SEED  RANGE  UNDEFINEDVALUE  TOLERANCE
    1     1e19     -2.5         1.0E-4     /
UDADIMS
20  /
--NOSIM

GRID      ============================================================

INIT
DX
  10.41667 3*333.3333 10.41667  /
DY
  5*100   /
DZ
  5*50   /
PERMX
  5*100   /
COPY
 PERMX  PERMY  /
 PERMX  PERMZ  /
/
MULTIPLY
PERMZ 0.1 /
/
PORO
  5*0.20   /
TOPS
  5*2600 /

PROPS     ============================================================
LSALTFNC
0.0     1  1*
3.7     1  1*
10.8     0  1*
30.0    0  1*
/
/
/
/
/
/
/
/
SWOF
-- SL = SWCR = 0.2   High salinity curves
```

```
-- Sw   Krw   Pwo
0.2     0.0000000       1.0000000       0
0.22    0.0006612       0.8948279       0
0.24    0.0026446       0.7973013       0
0.26    0.0059504       0.7071315       0
0.28    0.0105785       0.6240301       0
0.3     0.0165289       0.5477085       0
0.32    0.0238017       0.4778783       0
0.34    0.0323967       0.4142509       0
0.36    0.0423140       0.3565379       0
0.38    0.0535537       0.3044508       0
0.4     0.0661157       0.2577010       0
0.42    0.0800000       0.2160000       0
0.44    0.0952066       0.1790594       0
0.46    0.1117355       0.1465905       0
0.48    0.1295868       0.1183050       0
0.5     0.1487603       0.0939144       0
0.52    0.1692562       0.0731300       0
0.54    0.1910744       0.0556634       0
0.56    0.2142149       0.0412261       0
0.58    0.2386777       0.0295297       0
0.6     0.2644628       0.0202855       0
0.62    0.2915702       0.0132051       0
0.64    0.3200000       0.0080000       0
0.66    0.3497521       0.0043817       0
0.68    0.3808264       0.0020616       0
0.7     0.4132231       0.0007513       0
0.72    0.4469421       0.0001623       0
0.74    0.4819835       0.0000060       0
0.75    0.5000000       0.0000000       0       /

-- low salinity
-- Sw   Krw                     Kro
0.15    0.0000000       1.0000000       0
0.17    0.0002489       0.9221144       0
0.19    0.0009956       0.8483816       0
0.21    0.0022400       0.7786880       0
0.23    0.0039822       0.7129197       0
0.25    0.0062222       0.6509630       0
0.27    0.0089600       0.5927040       0
0.29    0.0121956       0.5380290       0
0.31    0.0159289       0.4868243       0
0.33    0.0201600       0.4389760       0
0.35    0.0248889       0.3943704       0
0.37    0.0301156       0.3528936       0
0.39    0.0358400       0.3144320       0
0.41    0.0420622       0.2788717       0
0.43    0.0487822       0.2460990       0
0.45    0.0560000       0.2160000       0
0.47    0.0637156       0.1884610       0
0.49    0.0719289       0.1633683       0
0.51    0.0806400       0.1406080       0
0.53    0.0898489       0.1200664       0
0.55    0.0995556       0.1016296       0
0.57    0.1097600       0.0851840       0
0.59    0.1204622       0.0706157       0
0.61    0.1316622       0.0578110       0
0.63    0.1433600       0.0466560       0
0.65    0.1555556       0.0370370       0
0.67    0.1682489       0.0288403       0
0.69    0.1814400       0.0219520       0
0.71    0.1951289       0.0162584       0
0.73    0.2093156       0.0116456       0
0.75    0.2240000       0.0080000       0
0.77    0.2391822       0.0052077       0
0.79    0.2548622       0.0031550       0
0.81    0.2710400       0.0017280       0
0.83    0.2877156       0.0008130       0
0.85    0.3048889       0.0002963       0
0.87    0.3225600       0.0000640       0
0.89    0.3407289       0.0000024       0
0.90    0.3500000       0.0000000       0       /
-- High Salinity Curves Table 3
0.2             0               1               0
0.215691        0               0.992761        0
0.241445        0               0.970257        0
```

```
0.268136        0               0.936997        0
0.295119        0               0.895909        0
0.322232        0               0.849797        0
0.34942         0               0.800541        0
0.376661        0               0.749224        0
0.403926        0               0.698169        0
0.431211        0               0.648925        0
0.45851         0               0.602028        0
0.485824        0               0.558066        0
0.513148        0               0.517143        0
0.540481        0.000001        0.479213        0
0.567821        0.000015        0.444253        0
0.593905        0.03922         0.375449        0
0.608131        0.241542        0.157734        0
0.615301        0.296463        0.084126        0
0.620255        1*              0.058508        0
0.624209        1*              0.045858        0
0.627561        1*              0.037976        0
0.630525        1*              0.032846        0
0.63319         1*              0.028841        0
0.635607        1*              0.025678        0
0.637825        1*              0.023232        0
0.639888        1*              0.02141         0
0.64183         1*              0.019984        0
0.643657        0.304882        0.018669        0
0.645373        1*              0.017486        0
0.646985        1*              0.016445        0
0.648503        1*              0.015555        0
0.649938        1*              0.014812        0
0.651299        1*              0.014182        0
0.6526          1*              0.013658        0
0.653852        1*              0.013243        0
0.655062        1*              0.012887        0
0.656231        1*              0.012501        0
0.657356        1*              0.012094        0
0.658438        1*              0.011677        0
0.659477        0.305077        0.01126         0
0.75            0.5             0               0       /

-- High Salinity Curves Table 4
0.2             0               1               0
0.201371        0.000005        0.998827        0
0.214502        0.000006        0.99238         0
0.234694        0.000006        0.973331        0
0.257104        0.000006        0.942801        0
0.280517        0.000006        0.903482        0
0.304536        1*              0.857955        0
0.328945        1*              0.808584        0
0.353655        1*              0.757622        0
0.378617        1*              0.706649        0
0.40378         1*              0.656934        0
0.4291          0.000006        0.609361        0
0.454544        1*              0.564552        0
0.480106        1*              0.522738        0
0.505781        1*              0.483947        0
0.531562        0.000006        0.448159        0
0.557405        0.00112         0.414333        0
0.577266        0.147327        0.247363        0
0.585849        0.267026        0.110562        0
0.590738        0.288175        0.071163        0
0.594289        1*              0.054529        0
0.597186        1*              0.045459        0
0.59967         1*              0.039352        0
0.601883        1*              0.035123        0
0.60392         1*              0.032156        0
0.605824        1*              0.029705        0
0.607605        1*              0.027586        0
0.609277        1*              0.02577         0
0.610852        1*              0.024231        0
0.612345        0.288942        0.02295         0
0.613767        1*              0.021911        0
0.615131        1*              0.021096        0
0.616451        1*              0.020496        0
0.617736        1*              0.020064        0
0.618989        1*              0.01963         0
0.620191        1*              0.019151        0
```

```
0.621351        1*              0.018651        0
0.622463        1*              0.01814         0
0.623529        1*              0.017628        0
0.624552        1*              0.017123        0
0.75            0.5             0               0       /

-- High Salinity Curves Table 5
0.2             0               1               0
0.206556        0.000016        0.994335        0
0.224026        1*              0.970859        0
0.245254        1*              0.925451        0
0.267872        1*              0.864436        0
0.291187        1*              0.794867        0
0.314959        1*              0.722924        0
0.339049        1*              0.652497        0
0.36336         1*              0.586252        0
0.387852        0.000016        0.525705        0
0.41251         1*              0.471231        0
0.437322        1*              0.422786        0
0.462271        1*              0.379993        0
0.487342        1*              0.34241 0
0.51252         1*              0.309457        0
0.537789        1*              0.280471        0
0.562193        0.018191        0.238581        0
0.575429        0.147487        0.10928 0
0.581273        0.198994        0.063447        0
0.584729        0.216388        0.049585        0
0.587424        0.226323        0.042373        0
0.589686        0.23287         0.038075        0
0.591656        0.237829        0.035019        0
0.593426        0.241752        0.032782        0
0.595058        0.244964        0.031122        0
0.596598        0.247679        0.029889        0
0.598061        0.250155        0.028822        0
0.599453        0.252497        0.027812        0
0.600776        0.25471         0.026859        0
0.602036        0.256801        0.025964        0
0.603236        0.258764        0.025129        0
0.60438         0.260624        0.024355        0
0.605473        0.26237         0.023644        0
0.606516        0.26402         0.022997        0
0.75            0.5             0               0       /

-- Low salinity curves Table 6
0.15    0       1       0
0.162046        0       0.996334        0
0.18681 0       0.982042        0
0.213149        0       0.958945        0
0.239941        0       0.929482        0
0.266937        0       0.894669        0
0.294044        0       0.856198        0
0.321214        0       0.814552        0
0.34843 0       0.772021        0
0.375672        0       0.729501        0
0.402936        0       0.687483        0
0.430218        0       0.64681 0
0.457515        0       0.607719        0
0.484824        0       0.570466        0
0.512139        0       0.535304        0
0.539461        0       0.502085        0
0.566787        0       0.470957        0
0.594119        0       0.442128        0
0.621455        0       0.415326        0
0.648794        0       0.390192        0
0.676138        0.000001        0.366948        0
0.703427        0.001522        0.343945        0
0.725307        0.111603        0.220637        0
0.735666        0.225107        0.096783        0
0.741695        0.250141        0.058811        0
0.746144        1*      0.043331        0
0.749806        1*      0.03503 0
0.75298 1*      0.029652        0
0.755826        1*      0.025965        0
0.758416        1*      0.023054        0
0.760798        1*      0.020766        0
0.763017        1*      0.018999        0
```

```
0.765106        1*      0.017572        0
0.767076        1*      0.016288        0
0.768933        1*      0.015151        0
0.77069 1*      0.01416 0
0.77185 0.253557        1*      0
0.772356        1*      0.013311        0
0.773945        1*      0.012597        0
0.775467        1*      0.012012        0
0.776934        1*      0.011529        0
0.778347        1*      0.011065        0
0.779706        1*      0.010625        0
0.781011        1*      0.010214        0
0.782265        1*      0.009836        0
0.78347 1*      0.009492        0
0.784629        1*      0.009175        0
0.785747        1*      0.008882        0
0.786825        1*      0.008616        0
0.78787 1*      0.008379        0
0.788885        1*      0.008174        0
0.9     0.35    0       0       /

 -- Low salinity curves Table 7
        0.15    0       1       0
0.155658        0.000002        0.998165        0
0.172661        0.000002        0.990286        0
0.193997        0.000002        0.973749        0
0.216915        0.000002        0.949391        0
0.240622        0.000002        0.918574        0
0.26482 1*      0.882848        0
0.289346        1*      0.843499        0
0.314131        1*      0.8021  0
0.339125        1*      0.759559        0
0.364282        1*      0.717006        0
0.389571        1*      0.675148        0
0.414982        1*      0.634557        0
0.440506        1*      0.595617        0
0.454359        0.000002        1*      0
0.466133        1*      0.558674        0
0.491851        1*      0.523831        0
0.517648        1*      0.490991        0
0.543514        1*      0.460424        0
0.569436        1*      0.431819        0
0.595414        1*      0.40535 0
0.621448        1*      0.380691        0
0.647537        1*      0.35783 0
0.673634        0.001161        0.335602        0
0.694818        0.101164        0.222099        0
0.704476        0.214919        0.098271        0
0.709711        0.240032        0.060351        0
0.713401        1*      0.045206        0
0.716356        1*      0.037221        0
0.718885        1*      0.032104        0
0.721126        1*      0.028547        0
0.723172        1*      0.025998        0
0.725067        1*      0.023903        0
0.726833        1*      0.022135        0
0.728491        1*      0.020649        0
0.73006 1*      0.019404        0
0.731556        1*      0.018371        0
0.732469        0.243172        1*      0
0.732996        1*      0.017521        0
0.734393        1*      0.016832        0
0.73575 1*      0.016198        0
0.737068        1*      0.015601        0
0.738343        1*      0.015044        0
0.739578        1*      0.014529        0
0.740772        1*      0.014058        0
0.741927        1*      0.013633        0
0.743044        1*      0.013255        0
0.744125        1*      0.012922        0
0.745174        1*      0.012623        0
0.746191        1*      0.012351        0
0.9     0.35    0       0       /

-- Low salinity curves Table 8
0.15    0       1       0
```

```
0.155484        0.000006        0.996724        0
0.172077        0.000006        0.982415        0
0.193137        1*      0.952208        0
0.215783        1*      0.908895        0
0.239199        1*      0.856321        0
0.263074        1*      0.798636        0
0.287264        1*      0.738665        0
0.311673        1*      0.679343        0
0.336259        1*      0.622364        0
0.361   1*      0.568829        0
0.385875        1*      0.519272        0
0.410866        1*      0.474048        0
0.435956        1*      0.433017        0
0.461129        1*      0.39587 0
0.48637 1*      0.362558        0
0.499422        1*      1*      0
0.511676        1*      0.332552        0
0.537046        1*      0.305698        0
0.56248 1*      0.281547        0
0.587978        1*      0.259835        0
0.613537        1*      0.240332        0
0.639155        1*      0.222774        0
0.664803        0.00042 0.206552        0
0.686291        0.053864        0.143719        0
0.696068        0.13423 0.066014        0
0.701049        0.160834        0.042293        0
0.704239        0.170991        0.033952        0
0.706793        0.177   0.029367        0
0.708959        0.18102 0.026525        0
0.710854        0.184042        0.024509        0
0.71256 0.186397        0.02305 0
0.714131        0.188297        0.021977        0
0.715597        0.189957        0.021082        0
0.716973        0.191463        0.020287        0
0.718271        0.19283 0.01958 0
0.719504        0.194093        0.01895 0
0.720683        0.195252        0.018389        0
0.721815        0.196322        0.017892        0
0.722909        0.197315        0.017452        0
0.723973        0.198239        0.017071        0
0.725012        0.199099        0.016743        0
0.726034        0.199925        0.016493        0
0.727041        0.200679        0.016217        0
0.9     0.35    0       0       /

PVDO
  200    1.0     0.47
  280    0.999   0.47
  300    0.998   0.47
/
ROCK
 270 .3E-5 /
DENSITY
-- o    w    g
 850. 1000. 1.2 /
PVTWSALT
 270.0 0.0/
 0.0  1.030  4.6E-5  0.5  0.0
10.0  1.030  4.6E-5  0.5  0.0 /

REGIONS    ============================================================

SATNUM
-- immiscible, high salinity = 1
 1 3 4 5 1
/
LWSLTNUM
-- low salinity curves
 2 6 7 8 2
/
RPTREGS
 24*0 /
RPTREGS
SURFNUM LWSLTNUM LSLTWNUM /

SOLUTION   ============================================================
```

```
EQUIL
-- Datum   Pressure   WOC
2680       270        2680 1*  2000/
SALTVD
 5000.0  30.0
 5500.0  30.0 /
RPTRST
'BASIC=2'  /

SUMMARY    ============================================================
FSPR
FSPT
FSIR
FSIT
FWIR
FOPR
FGPR
FOPT
FPR
FOPV
FWIT
FOE
TCPU
GSPR
 'G' /
GSPT
 'G' /
GSIR
 'G' /
GSIT
 'G' /
GSPR
 'G' /
WSPR
 'OP' /
WSPT
 'OP' /
WSIR
'INJ' /
WSIT
'OP ' /
WBHP
/
WOPR
'OP' /
WGPR
'OP' /
WLPR
'OP' /
WWPR
'OP' /
WWCT
'OP' /
WWIR
'INJ'/
CSFR
 'OP'   5 1 1 /      con. salt flow rate (+/-)
 'INJ'  1 1 1 /
/
CSPT
 'OP'  5 1 1 /
/
CSIT
 'INJ'  1 1 1 /
/
BSCN
 1 1 1 /
 2 1 1 /
 3 1 1 /
 4 1 1 /
 5 1 1 /
/
BSIP
 1 1 1 / salt in place
 2 1 1 /
 3 1 1 /
```

```
 4 1 1 /
 5 1 1 /
/
BPR
 1 1 1 /
 2 1 1 /
 3 1 1 /
 4 1 1 /
 5 1 1 /
/
BOSAT
 1 1 1 /
 2 1 1 /
 3 1 1 /
 4 1 1 /
 5 1 1 /
/
BGSAT
 1 1 1 /
 2 1 1 /
 3 1 1 /
 4 1 1 /
 5 1 1 /
/
BWSAT
 1 1 1 /
 2 1 1 /
 3 1 1 /
 4 1 1 /
 5 1 1 /
/
BWVIS
 1 1 1 /
 2 1 1 /
 3 1 1 /
 4 1 1 /
 5 1 1 /
/
BOKR
 1 1 1 /
 2 1 1 /
 3 1 1 /
 4 1 1 /
 5 1 1 /
/
BGKR
 1 1 1 /
 2 1 1 /
 3 1 1 /
 4 1 1 /
 5 1 1
/
BWKR
 1 1 1 /
 2 1 1 /
 3 1 1 /
 4 1 1 /
 5 1 1 /
/
BWKR
 1 1 1 /
 2 1 1 /
 3 1 1 /
 4 1 1 /
 5 1 1 /
/
FUHCPVI
RPTONLY
ALL
SEPARATE
RUNSUM
MSUMLINS
MSUMNEWT

SCHEDULE    ============================================================
```

```
TUNING
1 30 /
 /
 /
WELSPECS
'OP'   'G'   5  1  2600  'OIL'  /
'INJ'  'G'   1  1  2600  'WAT'  /
/
COMPDAT
'OP      '   5    1   1   1  'OPEN'   0  .0   157E-3 /
'INJ     '   1    1   1   1  'OPEN'   0  .0   157E-3 /
/
WCONPROD
'OP' 'OPEN' 'RESV' 4* 304.8 0.0 7* /
/
WCONINJE
'INJ'  'WAT' 'OPEN' 'RESV' 1* 304.8 /
/
UDQ
DEFINE FUHCPV FOPV /
UPDATE FUHCPV NEXT /
/
WCONPROD
'OP' 'OPEN' 'RESV' 4* 304.8 0.0 7* /
/
WCONINJE
'INJ'  'WAT' 'OPEN' 'RESV' 1* 304.8 /
/
UDQ
DEFINE FUHCPVI FWIT/FUHCPV /
/
WSALT
INJ 1 /
/
TSTEP
228*30 /

END
```